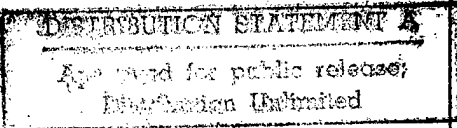


## REPORT DOCUMENTATION PAGE

0683

Public reporting burden for this collection of information is estimated to average 1 hour per response, including gathering and maintaining the data needed, and completing and reviewing the collection of information. Send comments regarding this burden estimate or any aspect of this collection of information, including suggestions for reducing this burden, to Washington Headquarters Service, Directorate for Information Operations and Reports, 1215 Jefferson Davis Highway, Suite 1204, Arlington, VA 22202-4302, and to the Office of Management and Budget, Paperwork Reduction Project (0704-0188), Washington, DC 20503.

1. AGENCY USE ONLY (Leave blank)		2. REPORT DATE 09-21-98	3. REPORT TYPE AND DATES COVERED Final 09-30-95 to 09-30-98	
4. TITLE AND SUBTITLE High Bandwidth Optical Switching Technology for Optical Fiber Communication			5. FUNDING NUMBERS F49620-95-C-0077	
6. AUTHOR(S) Ravinder Kachru				
7. PERFORMING ORGANIZATION NAME(S) AND ADDRESS(ES) SRI International 333 Ravenswood Avenue Menlo Park, CA 94025-3493			8. PERFORMING ORGANIZATION REPORT NUMBER PYU 7509	
9. SPONSORING/MONITORING AGENCY NAME(S) AND ADDRESS(ES) Air Force Office of Scientific Research Directorate of Physics and Electronics/AFOSR 110 Duncan Avenue, Suite B115 Bolling AFB, DC 20332			10. SPONSORING/MONITORING AGENCY REPORT NUMBER	
11. SUPPLEMENTARY NOTES				
12a. DISTRIBUTION/AVAILABILITY STATEMENT Distribution unlimited.				12b. DISTRIBUTION CODE
13. ABSTRACT (Maximum 200 words)  While fiber optic technology has the intrinsic high bandwidth for the backbone transmission required of a high speed communications network, the creation of the high bandwidth network to users remains a challenge. The main impediment thus far to the development of a high speed optical network has been the absence of the following key technologies: (1) a high speed optical memory, (2) optical header recognition, (3) high speed switching commensurate with the high data capacity of an optical fiber, and (4) integration and expansion of the above functions by wavelength division multiplexing (WDM) and code-division multiple-access (CDMA). No technologies that have all four of these critical elements are currently available.  SRI is developing a high speed fiber optic communication network based on asynchronous transfer mode (ATM). The proposed system combines optics, electronics, and software. These techniques will allow us to route, distribute, and prioritize messages without ever performing optical-to-electrical conversions at the data bit rate. Electronic operations can be confined to the much slower				
14. SUBJECT TERMS Optical memories Digital holographic memory Optical cache memory			Optical data Optical packet decoding	Recording High speed memory
			15. NUMBER OF PAGES	
			16. PRICE CODE	
17. SECURITY CLASSIFICATION OF REPORT UNCLASSIFIED	18. SECURITY CLASSIFICATION OF THIS PAGE UNCLASSIFIED	19. SECURITY CLASSIFICATION OF ABSTRACT UNCLASSIFIED	20. LIMITATION OF ABSTRACT Unlimited	

technology can be considered commercially viable, such as the low operating temperature currently used, which will require further efforts in the development of high-temperature storage materials.

## REFERENCES AND NOTES

1. D. Psaltis and F. Mok, *Sci. Am.* **273**, 70 (November 1995).
2. J. F. Heanue, M. C. Bashaw, L. Hesselink, *Science* **265**, 749 (1994).
3. M. P. Bernal *et al.*, *MRS Bull.* **21**, 51 (1996).
4. E. S. Maniloff *et al.*, *Appl. Opt.* **34**, 4140 (1995).
5. T. W. Mossberg, *Opt. Lett.* **7**, 77 (1982).
6. X. A. Shen, E. Chiang, R. Kachru, *ibid.* **19**, 1246 (1994).
7. T. Mossberg, R. Kachru, S. R. Hartmann, A. Flusberg, *Phys. Rev. A* **20**, 1976 (1979); V. V. Samartsev, R. G. Usmanov, G. M. Ershov, B. Sh. Khamidullin, *Sov. Phys. JETP* **47**, 1030 (1978); V. A. Zulkov, V. V. Samartsev, R. G. Usmanov, *JETP Lett.* **32**, 270 (1980); J. B. W. Morsink, W. H. Hesselink, D. A. Wiersma, *Chem. Phys. Lett.* **64**, 1 (1979).
8. The fundamental difference between the present technique and the persistent spectral hole-burning (PSHB) holographic recording [see, for example, A. Renn *et al.*, *J. Lumin.* **38**, 37 (1987)] is that in PSHB, the sample is exposed simultaneously to two laser beams and a spectral hole is burned at the laser wavelength. The depth of the hole at a given spatial location varies according to the spatial interference pattern generated by both beams, and no temporal information is recorded in the holograms. These holograms are known as volume holograms, identical to those obtained in photorefractive memories. The technique also differs significantly from the accumulated photon echo (APE) memory in that APE uses multiple pairs of write and data pulses to record a single image at one spectral location [P. Saari, R. Kaarli, A. Rebane, *J. Opt. Soc. Am. B* **3**, 527 (1986)].
9. R. Yano, M. Mitsunaga, N. Uesugi, *Opt. Lett.* **16**, 1884 (1991).
10. The SLM used in the present experiment is a liquid-crystal array taken from a commercial projection television. The array consists of 480 pixels by 440 pixels and has a fill factor of ~24%. This low fill factor introduces a large insertion loss in the transmitted beam. We measured the loss for the zeroth-order transmission to be ~97% at 580 nm. We chose a  $5 \times 5$  region of the SLM to represent a data bit and used a total of 3360 bits (60 bits by 56 bits) in each data frame to cover a center area equal to about 40% (~1.6 cm  $\times$  1.3 cm) of the SLM.
11. The length of the data pulse varied from 11.2 to 50  $\mu$ s. This pulse was biphasic-modulated with pseudo-random code [Y. S. Bai and R. Kachru, *Opt. Lett.* **18**, 1189 (1993)] to reduce coherent saturation as well as echo fluctuations caused by laser wavelength instability. The write and read pulses were 10- $\mu$ s-long square pulses with a peak power of only ~200 mW. These pulses were also biphasic-encoded but with the 5-bit Barker code [see, for example, M. N. Cohen, in *Principles of Modern Radar*, J. L. Eaves and E. K. Reedy, Eds. (Van Nostrand Reinhold, New York, 1987), p. 465] to increase the data channel width to ~500 kHz. Such an increase of channel width makes the memory system more tolerant to laser wavelength instability and hence reduces the fluctuation of echo intensity.
12. To achieve the required frequency precision, we used a Coherent ring dye laser and further frequency-stabilized the laser by using the Pound-Drever-Hall method [R. W. P. Drever *et al.*, *Appl. Phys. B* **31**, 97 (1983)]. By using an intracavity electro-optic modulator and locking the laser to an external reference cavity, we substantially reduced laser noise with frequencies above ~1 kHz and achieved a laser linewidth with respect to the cavity of ~40 kHz over a time period of 20 ms. We accomplished WDM by tuning the laser externally with an acousto-optic modulator to achieve a channel access time of ~1  $\mu$ s.
13. For a detailed discussion on the advantages of using WDM in frequency-selective storage materials, see, for example, B. Kohler *et al.*, *Opt. Lett.* **18**, 2144 (1993).
14. D. Psaltis, D. Brady, K. Wagner, *Appl. Opt.* **27**, 1752 (1988).
15. The intensified CCD camera has an array of 768 pixels by 484 pixels. However, the frame grabber digitizes the captured images at a reduced horizontal resolution of 640 pixels per line. The data frame from the SLM is imaged (1:1) onto the CCD array, resulting in an average bit size of 10.7 pixels  $\times$  8.4 pixels after digitization. The mismatch between the frame grabber and CCD, and that between the CCD and SLM, as well as the low spatial resolution of the intensifier (~64 line pairs per millimeter), prevented the use of small bit dimensions. We used these mismatched devices because they were readily available and made no attempt to match their dimensions.
16. M. M. Wang *et al.*, *Opt. Lett.* **22**, 558 (1997).
17. This research was supported by the Defense Advanced Research Projects Agency (DARPA) under contract F49620-95-C-0077 and by Air Force Office of Scientific Research (AFOSR) under contract F49620-95-C-0029. Helpful suggestions and discussions with R. Leheny of DARPA and A. Craig of AFOSR are gratefully acknowledged.

27 May 1997; accepted 22 August 1997

CLASSIFIED BY:

N/A since Unclassified.

DECLASSIFY ON:

N/A since Unclassified.

## 13. ABSTRACT (Continued)

decisions and control operations that need to be made only once for each data packet. Thus, data throughput through a single router can be increased over the raw electronic processing speed by a factor equal to the number of bits in the packet, i.e., several orders of magnitude. We expect our concept to provide a user throughput in excess of 30 Gb/s and an overall network throughput in excess of  $10^{12}$  bits/s.

During the past three years, SRI International investigated many issues related to the practical development to an optical packet switch using rare-earth doped materials. Specifically SRI focused on three major research areas. (1) Investigating new rare-earth storage materials that can be used directly at communication wavelengths, specifically at 1.5  $\mu\text{m}$ . (2) Demonstrating optical packet buffering at this wavelength, building a compact demonstration unit using optical fiber input and output. (3) Examining the use of time-domain holography for massively parallel optical data buffering/storage and determining the data input/output transfer rate and BER of the system.

$\text{Er}^{3+}$ :YAG and  $\text{Er}^{3+}$ : $\text{Y}_2\text{SiO}_5$  have been identified as suitable candidates for data buffering at 1.5  $\mu\text{m}$ . The dephasing time has been measured as 50 ns for  $\text{Er}^{3+}$ :YAG and 120  $\mu\text{s}$  for  $\text{Er}^{3+}$ : $\text{Y}_2\text{SiO}_5$ , with the latter measurement obtained under a magnetic field of 6G. The material-limited time-bandwidth products for both materials are around 120,000, which suggests a potential storage density of 120 bit/focal spot. The storage time for three-pulse echoes has also been measured for the materials and is between 1 and 30 mn, depending upon the laser power used in recording and retrieval.

In a separate experiment using a 0.8-mm spot size (FWHM=0.8 mm), we successfully stored 1020 bits of data (306 ones and 714 zeros) in a 40 MHz channel spectral width. The total length of the data was 51  $\mu\text{s}$ , approximately 2/5 of the material's phase memory time. The retrieved data intensity, therefore, is expected to decay substantially (approximately one order of magnitude) over the length of the string. To prevent this fast decay, we swept the intensity of the input data exponentially upwards so that the entire data string can be resolved clearly on a single intensity scale with a good signal-to-noise ratio. Data recall can take place at any time after storage. This attribute made this technique also useful as a programmable optical delay line.

SRI has also demonstrated page-formatted data storage using the time-domain approach. One hundred pages of data, each of which contained 3,360 bits, have been recording in  $\text{Er}^{3+}$ : $\text{Y}_2\text{SiO}_5$  at a single spatial location by using wavelength multiplexing. The digital data were recorded and accurately retrieved at a peak rate of 300 Mbits per second without the use of an error correcting code. The system's bit error rate is about  $10^{-7}$ .

The experimental results from this project clearly demonstrate the practical feasibility of using hole burning materials for optical packet switching using the stimulated echo approach.

19981102 125

## CONTENTS

ABSTRACT .....	i
LIST OF FIGURES.....	iv
BACKGROUND.....	1
Optical Random Access Memory .....	2
Angular Routing, Switching, and Multicasting.....	2
RESULTS.....	5
Time Domain Materials at 1.5 $\mu\text{m}$ .....	5
All-Optical Dynamic Memory for Fiber Communications.....	9
Massively Parallel Time-Domain Optical Memory .....	10
The Storage System .....	10
Analysis of Page-Formatted Binary Data .....	13
System Performance and Projections.....	16
CONCLUSIONS AND RECOMMENDATION.....	19
REFERENCES.....	20
APPENDIX A: Optimization of Time-Domain Storage Density in the Presence of Excitation-Induced Spectral Diffusion	
APPENDIX B: Observation of Photon Echo in $\text{Er}^{3+}:\text{YAG}$ At 1.527 $\mu\text{m}$	
APPENDIX C: Time-Domain Holographic Digital Memory	

## FIGURES

1. Optical random access memory (ORAM).....	5
2. Optical routing switch. (a) General schematic; (b) source, read, write, and destination packet directions.....	6
3. Energy level diagram of $\text{Er}^{3+}:\text{YAF}$ for the ${}^4\text{I}_{15/2}$ and ${}^4\text{I}_{13/2}$ state.....	8
4. (a) Two-pulse echo intensity in $\text{Er}^{3+}:\text{YAG}$ at $\sim 7$ K under an external magnetic field of 100 G as a function of change of excitation pulse separation. Open circles are data and the solid line is a simple exponential fit. (b) Stimulated photon echo intensity in $\text{Er}^{3+}:\text{YAG}$ as a function of the separation between the second and the third excitation pulses. The results are obtained at $\sim 1$ K under an external magnetic field of 3000 G.....	10
5. Storage of 1020 bits of data. The string is the ASCII representation of "Time-Domain Holography, Dynamic Optical Memory, Reprogrammable Optical Delay Lines at 1.5 microns" encoded with the (1.7) code. An exponential intensity ramp is used to compensate to the large decrease of the intensity of the retrieved data over 50 $\mu\text{s}$ . The peak power is measured to be $\sim 0.25 \mu\text{W}$ . All of the data traces shown in this figure represent single recording and retrieval events and are detected by an avalanche photodiode module with a gain of $9.4 \text{ V}/\mu\text{W}$ at 1.55 $\mu\text{m}$ .....	13
6. (a) Input data image after transmitted through the $\text{Eu}^{3+}:\text{Y}_2\text{SiO}_5$ sample. (b) Reconstructed image after being stored in $\text{Eu}^{3+}:\text{Y}_2\text{SiO}_5$ for 200 $\mu\text{s}$ . (c) Image reconstructed under the same condition as that of (b) but with weak overall intensity. (d) Image reconstructed 5 minutes after the completion of recording. In (a)-(c), the data pulse length was 11.6 $\mu\text{s}$ , and that in (d) was 50 $\mu\text{s}$ . The former corresponds to an I/O rate of 300 megabits per second while the latter corresponds to 67 megabits per second. ....	16
7. (a) Histogram showing the intensity distributions of 0's and 1's that were retrieved from the time-domain memory. (b) Normalized histogram obtained after applying the local threshold technique. ....	17
8. (a) Digitized photograph displayed using its original binary data. (b) Same photograph obtained after the binary data being transferred to and then recalled back from the time-domain memory.....	20

## BACKGROUND

There is a growing demand for high throughput data networks in both military and commercial applications, such as distribution of intelligence information (data, images) for the military and communication of multimedia services (voice, video, image, and data) for the commercial sector. Low-cost desktop workstations with more than 100 MIPS of processing power are currently being used, and workstations with ~1000 MIPS will be available in a few years. The image-based interaction and collaboration applications running on these workstations will impose enormous demands on network capacity. For example, transmission of a single high density television (HDTV) channel requires a data rate in excess of 40 Mbits/s, even with compression. Networks of the next decade will need to support hundreds or even thousands of such users. It is clear that the gigabit network architectures being developed today will not be able to meet the capacity requirements in the next decade.

With fiber optics as the physical-layer technology, the limiting factor on the bandwidth of a network is not the transmission medium but the electronic and photonic devices at the end-points. A single-mode optical fiber operating at a wavelength in the neighborhood of 1550 nm has a capacity of approximately 25,000 GHz, while electronic processing speeds are limited to a few Gbits/s. This speed mismatch can be expected to prevail for a long time. This limitation led researchers to investigate all-optical networks, where the path between two communicating end-points does not involve conversion to electronic signals for processing.

If optical networks are to be used widely, packet switching will need to be supported, as well as methods for interconnection of these networks. Packet switching allows more efficient utilization of network capacity than circuit switching because of the statistical multiplexing of bursty users. More importantly, packet switching allows multiple upper-level protocols and services to share the same physical network paths concurrently. Such support for multiple concurrent traffic streams is an absolute requirement in interactive computing. In addition, a large number of local area and wide area networks in the military and commercial sectors will be packet switching networks to which future optical networks must be connected. Hence, from the Department of Defense's communication infrastructure standpoint, any practical long-term solution to the utilization of optical devices for networking must accommodate packet switching.

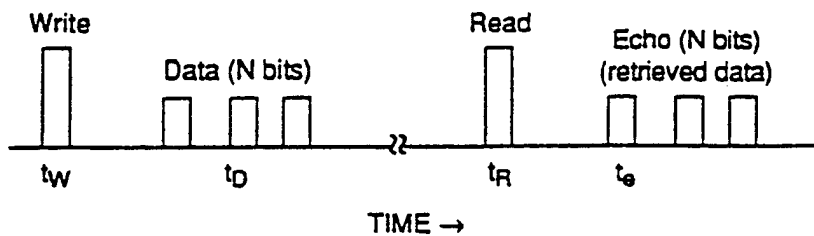
To illustrate the concept of optical switching using the stimulated echo concept, we use a simple diagram to describe the storage and retrieval of time domain data and then describe the switching aspects of this technique.

## OPTICAL RANDOM ACCESS MEMORY

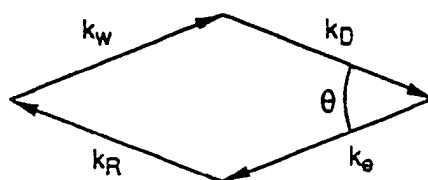
As shown in Figure 1a, information is written as phase/amplitude or frequency modulations by encoding the Data and Write laser beams, which cross inside the sample, at times  $t_D$  and  $t_w$ , respectively. The relative directions of the laser pulses are shown in Figure 1b. The overlap of these two beams causes the dopant materials, such as rare-earth ions doped in oxide crystals, to Fourier transform the time-domain data and store the information as a frequency grating at low temperatures. Information is retrieved sometime later by illuminating the crystal by a single Read pulse (which also may be modulated) at time  $t_R$ . The crystal then emits a laser-like coherent beam (the Echo beam) that is a replica of the original Data beam at time  $t_e = t_R + (t_D - t_w)$ . This random access memory can be dynamically configured with word sizes ranging from one bit up to  $10^6$  bits. Memory time of up to a day, memory density of  $10^{10}$  bits/cm<sup>3</sup>, and single pixel/channel I/O throughput in excess of 100 Mbits/s have been experimentally demonstrated. Figures 1c through 1e show the experimental storage and retrieval of 0.4 kbits of information in a single spatial spot in Eu:Y<sub>2</sub>SiO<sub>5</sub>. We have recently demonstrated storage of 2.0 kbits of data in a single spatial spot in Eu:Y<sub>2</sub>SiO<sub>5</sub>.

## ANGULAR ROUTING, SWITCHING, AND MULTICASTING

The storage medium stores not only the information carried by the Data and Write beams but also the relative angle of the beams. It can be shown that  $\vec{k}_{\text{echo}} = \vec{k}_D + \vec{k}_R - \vec{k}_w$ , where  $\vec{k}_{\text{echo}}$ ,  $\vec{k}_w$ ,  $\vec{k}_R$ , and  $\vec{k}_D$  are the propagation wave vectors of the retrieved data (Echo), Write, Read, and Data pulse train. This phase matching condition is exploited to produce angular routing, switching, and multicasting operation. Figure 2a shows a schematic outline of the optical routing switch. Figure 2b shows how buffered packet switching using the phase matching conditions discussed above can be accomplished. Assume that the packet exiting an input (source) fiber port  $i$  needs to be space-switched to an output (destination) port  $j$ . The destination port information is contained in the header information of the packet. This header information is optically decoded as discussed below and the output port determined. The Data and Write pulses intersect inside the sample at angle  $\pi - \theta$ . The destination port  $j$  is located at an angle  $\theta$  with respect to the source. The input packet emerging from the source fiber impinges on the crystal after passing through a fiber delay line. This data packet is first stored (buffered) in a particular physical location in the crystal by addressing the location first by a Write pulse and then by the data packet. This procedure stores not only the data packet information but also the destination angle  $\theta$ . The stored packet may be routed and switched out of the memory by addressing the memory location with a short Read pulse that travels opposite to the input packet. This Read pulse causes the memory to coherently emit (transmit) a packet (echo) that mimics the input data at an angle  $\theta$  with respect to the input data direction, as shown Figure 2b. The multicasting operation is easily accomplished by simultaneously sending two or more Write pulses at angles  $\theta_1$ ,  $\theta_2$ , and so on, during the recording. The packet thus stored can be readily switched to the predetermined destination(s) by using a single Read pulse.



(a) Temporal schematic of first-in-first-out (FIFO) data memory.



(b) One of the many possible relative directions of the write, data, read, and echo pulses.



(c) Input pulse sequence and echo signal. Full horizontal scale =  $102.4 \mu\text{s}$ . The duration of the data pulse is  $10 \mu\text{s}$  (400 bits). The input pulses are attenuated by  $\sim 10^{-4}$ .



(d) Input data pulse ( $P_2$ ) on an expanded time scale. Full horizontal scale =  $2.4 \mu\text{s}$ .

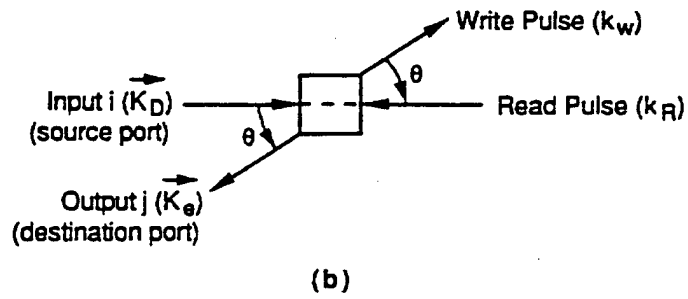
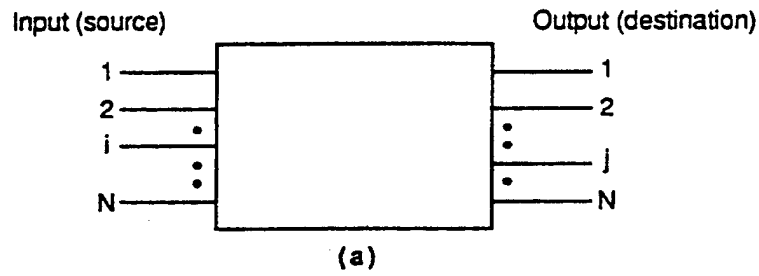


(e) Retrieved data pulse (echo) on an expanded time scale.

CAM-330581-167

Figure 1. Optical random access memory (ORAM).





CM-330581-168

Figure 2. Optical routing switch. (a) General schematic; (b) source, read, write, and destination packet directions.

## RESULTS

### TIME DOMAIN MATERIALS AT 1.5 $\mu\text{m}$

Unlike other optical memories, TDOM is a high-speed signal processor by nature. Temporal data strings stored at different times can be correlated or convoluted simultaneously with an incoming data string *in the memory* at bandwidths up to several GHz with no additional processing time required [1-8]. This rapid in-memory processing feature combined with the demonstrated high storage capacity makes TDOM also a superior candidate for applications ranging from high-speed optical packet switching, context-based retrieval, matched filtering, data encryption, to pattern recognition.

In spite of the rapid progress in the development of optical memories and all-optical processors, to our knowledge there exists no model directly operating at the optical communication wavelengths. The current optical devices require electrical to optical signal conversions which certainly reduce the data communication speed. To meet the rapidly increasing demand for high speed and high capacity optical communications, it becomes necessary to eliminate such electrical-optical conversions. However, it remains a challenge to find a suitable medium to store and process optical signals at the infrared wavelengths of fiber communication.

SRI has explored the feasibility of developing a TDOM that can be operated directly at the communication wavelengths. We choose the  ${}^4I_{15/2} - {}^4I_{13/2}$  transition in  $\text{Er}^{3+}:\text{YAG}$  as a candidate for the present study and examine some of its spectroscopic properties relevant to time-domain applications.

The erbium ion has an odd number of f-electrons, giving rise to Kramers degeneracy, which can only be lifted by external magnetic field. We resolved six lines associated with transitions from the lowest Stark level in the  ${}^4I_{15/2}$  state to six Stark levels of the  ${}^4I_{13/2}$  state (see Figure 3). Their wave numbers in order are 6549, 6599, 6606, 6786, 6806, and 6886  $\text{cm}^{-1}$ . The absorption line at 6527  $\text{cm}^{-1}$  at  $\sim 7$  K is a hotband from the second lowest Stark level ( $\sim 22$   $\text{cm}^{-1}$ ) in the  ${}^4I_{15/2}$  state to the lowest level of the  ${}^4I_{13/2}$  state. At higher temperature, we also observed hotband from higher Stark levels of the  ${}^4I_{13/2}$  state. The energy level diagram of  ${}^4I_{15/2}$  and  ${}^4I_{13/2}$  corresponding to our data is shown in Figure 3. Our results are in general consistent with earlier work on  $\text{Er}^{3+}:\text{YAG}$  by Ashurov and coworkers [9], who also observed only six lines for the  ${}^4I_{15/2} - {}^4I_{13/2}$  transition at 4 K. The data reported by Koningstein and Geusic [10] indicates an additional absorption line  $\sim 91$   $\text{cm}^{-1}$  above the highest line in our data, which may be too weak for us to detect.

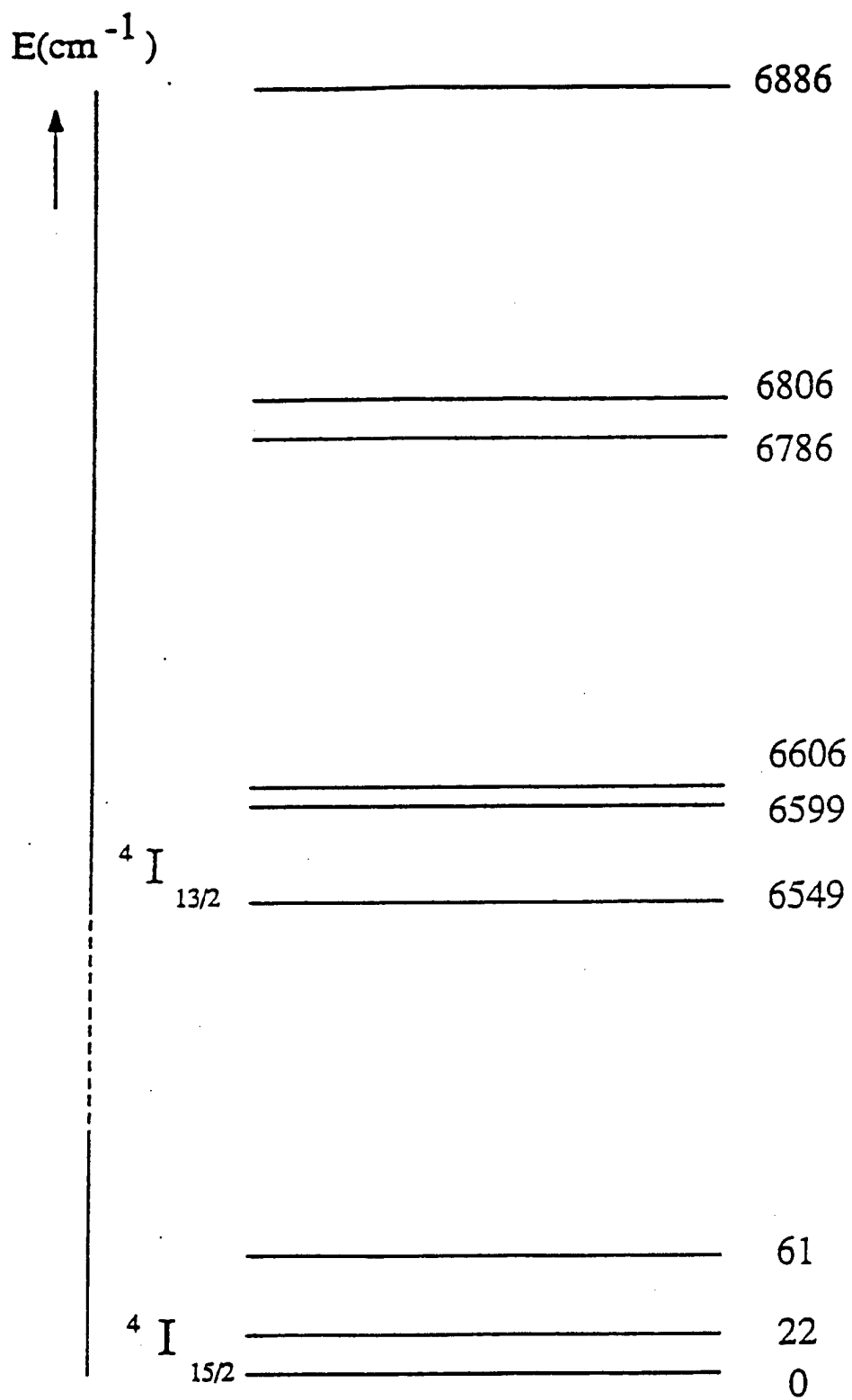


Figure 3. Energy level diagram of Er<sup>3+</sup>:YAF for the  $4I_{15/2}$  and  $4I_{13/2}$  state.

The inhomogeneous broadening of the transition was estimated to be ~20 GHz from the measured transmission spectrum. The homogeneous line width of this transition was measured by recording two-pulse echo intensity as a function of excitation pulse separation. A simple exponential fit to the data gives a homogeneous dephasing time  $T_2$  of ~50 ns. This dephasing time was found to vary little between 1 and 7 K under a magnetic field below 100 G.

In our two-pulse echo experiment, we used two dye lasers with 10 GHz spectral width. The peak intensity of the laser inside the crystal is about 1 MW/cm<sup>2</sup>. We use the fluorescence lifetime of the  $^4I_{13/2}$  excited state to calculate the laser pulse area [11] and take into account that the laser pulse is non-Fourier-transform-limited. The estimated pulse area is between  $\pi/8$  and  $\pi/4$ . This area of <1 was also supported by the experimental observation that the echo intensity was linear to the first laser pulse's intensity and quadratic to the second. We also found that reducing the laser power by a factor of 2 had no effect on the decay rate of the echo.

The data in Figure 4a were taken with an external magnetic field of ~100 G applied along the c-axis of the crystal. When this external field was raised from zero to 10 G, the echo intensity quickly increased by a factor of three. But this increase became saturated when the field was above 30 G. On the other hand the dephasing time did not change upon increasing the magnetic field to 100 G. When a magnetic field of ~3000 G was applied to the crystal (perpendicular to its c-axis), we observed apparently non-exponential decay of echo, but the dephasing time was not lengthened either.

One of the important parameters governing the performance of the time-domain memory is the highest temperature at which the storage sample can be operated. To determine this temperature, we measured two-pulse echo intensity at different sample temperatures. At a fixed excitation pulse separation about 35 ns, the echo intensity gradually decreased by only a factor of two from 7 to 11 K. In comparison to many other rare-earth doped crystals except  $\text{Eu}^{3+}:\text{Y}_2\text{SiO}_5$  at its  $^7F_0-^5D_0$  transition [12], this temperature dependence of  $\text{Er}^{3+}:\text{YAG}$  is considerably weaker.

In addition to the two-pulse echo experiments, we also examined three-pulse (or stimulated) photon echo in  $\text{Er}^{3+}:\text{YAG}$  since it is closely related to the physical processes involved in TDOM and related optical processors. By doing so, we would be able to estimate the potential performance of  $\text{Er}^{3+}:\text{YAG}$  as TDOM at 1.527  $\mu\text{m}$ , such as the maximum storage time, which is often limited by spectral diffusion resulting from ion-host and ion-ion interactions. We carried out the three-pulse stimulate echo experiment under a condition very similar to the two-pulse echo experiment. We fixed the separation between the first two excitation pulses at 20 ns and varied that between the second and the third pulses. The results (shown in Figure 4b) show a complicated decay feature, with an initial fast decay, followed by a slower decay and then another fast decay. At a delay of 50  $\mu\text{s}$ , the echo intensity decreased by a factor of 10 from that at 1  $\mu\text{s}$ .

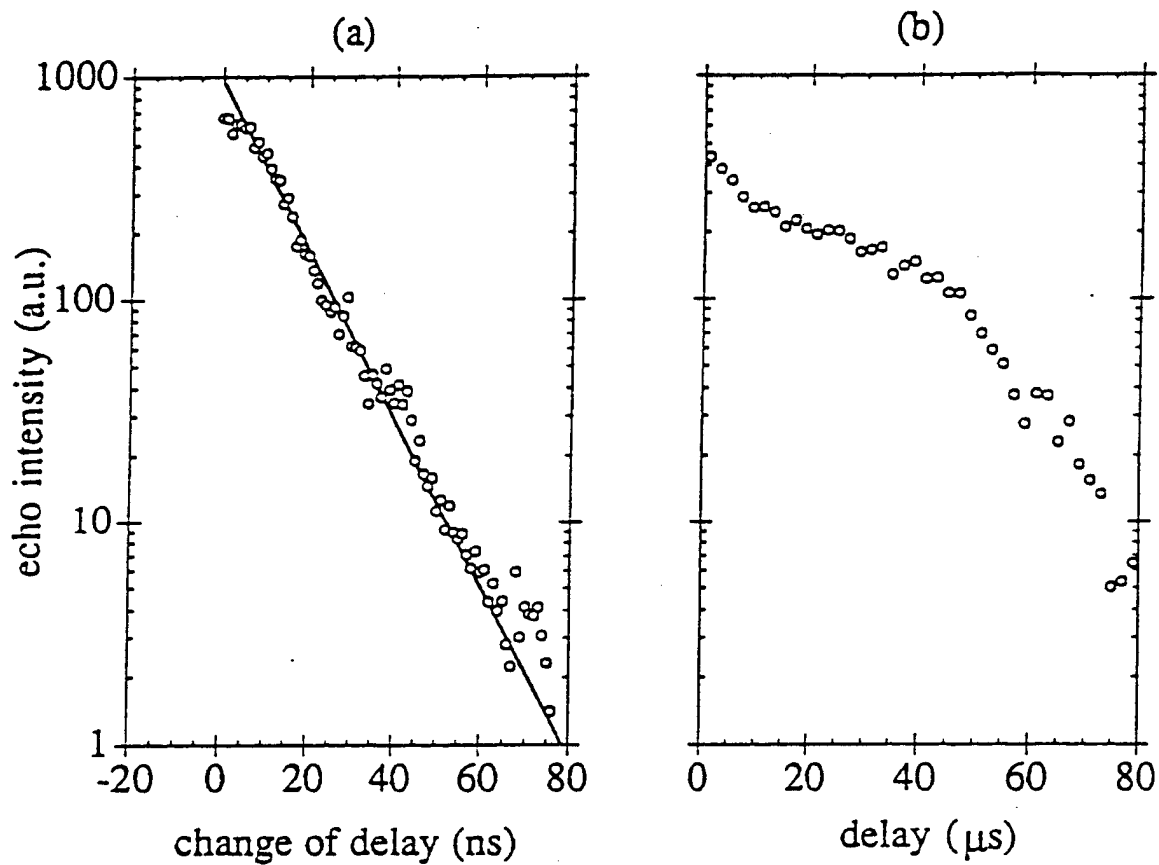


Figure 4. (a) Two-pulse echo intensity in  $\text{Er}^{3+}:\text{YAG}$  at  $\sim 7$  K under an external magnetic field of 100 G as a function of change of excitation pulse separation. Open circles are data and the solid line is a simple exponential fit. (b) Stimulated photon echo intensity in  $\text{Er}^{3+}:\text{YAG}$  as a function of the separation between the second and the third excitation pulses. The results are obtained at  $\sim 1$  K under an external magnetic field of 3000 G.

This decay is much faster than the fluorescence lifetime measured earlier, suggesting the presence of rapid spectral diffusion on a microsecond time scale. One possible cause of this fast diffusion is the strong Er-Er dipolar interactions as suggested by Macfarlane et al. [13].

In conclusion, we observed for the first time two-pulse and three-pulse echoes at 1.527  $\mu\text{m}$  in  $\text{Er}^{3+}$ :YAG. The fast dephasing together with its insensitivity to external magnetic field observed in our experiments, although less desirable, pose no significant challenge to the implementation of  $\text{Er}^{3+}$ :YAG as a time-domain storage medium in most of applications. For example, recently developed swept-carrier technique allows the storage of data strings that are much longer than the dephasing time of a storage material. The lifetime of the spectral grating measured by three-pulse echoes, although short, is still adequate for applications such as dynamic optical memory, optical packet buffering, and optical signal processing. The present work opens up the possibility of developing TDOM and TDOM-based optical processors operated directly at the communication wavelengths. Further improvement of material properties, such as longer dephasing time and less spectral diffusion, may be accomplished by choosing, e.g., different host materials, reducing Er concentrations, and/or applying larger external magnetic fields. These efforts have shown success in other rare-earth ions such as Eu and Pr ions. However, they may not be applicable to Er ions.

## ALL-OPTICAL DYNAMIC MEMORY FOR FIBER COMMUNICATIONS

In time-domain optical memory, temporal information is stored as spectral interference patterns in an inhomogeneously broadened electronic transition of rare-earth ions by resonant excitations. The interference patterns (referred to as spectral gratings) are generated by using a reference pulse known as the write pulse, which interferes in time-domain or equivalently in spectral domain, with the data sequence to be stored. Each bit of information is recorded as an integral part of the spectral gratings which extends over a spectral region determined by the data modulation bandwidth. These gratings in a carefully chosen material can persist for several hours to perhaps several days at cryogenic temperatures because the recorded information is actually stored as population modulation of hyperfine levels in the ground state. The maximum bandwidth of a data string is limited by the inhomogeneous linewidth of an electronic transition to be used, which for rare-earth doped solids, is typically between 1.0 and 10 GHz.

Temporal information recorded in the memory is retrieved by illuminating the spectral gratings with a read pulse, which induces coherent radiation known as photon echoes. In order for the echo to mimic the temporal data string originally stored, the product of the Fourier transforms of the write and read pulses must be spectrally flat over the bandwidth of the data string. This feature of rapidly recording optical information in a bit-serial format distinguishes the time-domain memory from other optical storage techniques, such as photorefractive and persistent spectral holeburning memories, where serial data must be first converted to parallel ones before recording can take place.

Storage of 1020 bits of data is shown in Figure 5. The storage material is  $\text{Er}^{3+}:\text{Y}_2\text{SiO}_5$  (0.005 at. % and 7 mm thick). Optical information is stored in the  ${}^4\text{T}_{15/2} - {}^4\text{T}_{13/2}$  transition of the crystal, which has two optically equivalent sites, one at 1.5364  $\mu\text{m}$  (site 1) and the other at 1.5388  $\mu\text{m}$  (site 2). Each optical site has an inhomogeneous broadening of  $\sim 1$  gigahertz. To increase the length of a data string that can be stored each time (which is determined by the phase memory time of the transition), we place the sample between two permanent magnets with a magnetic field ( $\sim 3$  kilogauss) perpendicular to the optical beam axis.

A number of issues still need to be addressed before such a dynamic memory can be built. One of them is how to tailor the gain of the optical amplifier so that the retrieved optical waveforms are identical to the input to maintain the signal fidelity over a large of refreshing cycles. This may be accomplished by saturating the gain medium of the optical amplifier, for example.

## MASSIVELY PARALLEL TIME-DOMAIN OPTICAL MEMORY

Time-domain holographic memory has emerged as an excellent candidate for such I/O intensive applications. This memory possesses not only features that are common to conventional spatial holographic recording, such as high capacity and high degree of parallelism, but also those that are unique and complementary to the conventional holography. The most appealing one is its fast page recording speed under a modest laser power. Recent experiments [7] show that an exposure time of several microseconds and a peak laser power of less than 200 mW are sufficient to record a high-resolution binary image with the time-domain technique.

The spectral interference of the two pulses is recorded in a storage medium (which are often rare-earth doped solids such as  $\text{Eu}^{3+}:\text{Y}_2\text{SiO}_5$  or  $\text{Pr}^{3+}:\text{YAG}$ ) by laser excitation. Ions such as  $\text{Eu}^{3+}$  and  $\text{Pr}^{3+}$  that are responsible for data recording are resonantly excited by the laser pulses to form population gratings resembling the Fourier spectra of the pulse pair. These gratings in a carefully chosen material can persist for several hours to perhaps several days at cryogenic temperatures because the recorded information is actually stored as population modulation of hyperfine levels in the ground state [7]. Since the grating is a direct result of resonant excitation and requires no secondary process, its formation is instantaneous and requires modest laser power, the data recording is therefore inherently fast and efficient, giving rise to high data transfer rates, fast access times, and short latency. These features are ideal for applications as a dynamic memory.

**The storage system.** The material chosen to demonstrate this novel holographic recording scheme is crystalline  $\text{Eu}^{3+}:\text{Y}_2\text{SiO}_5$  (0.1 at. % and 7 mm thick). We use its  ${}^7\text{F}_0 - {}^5\text{D}_0$  transition at Site 1 ( $\sim 579.88$  nm) which has an inhomogeneously broadened linewidth of  $\sim 4$  GHz and a dephasing time of  $\sim 2$  ms. The product of the two parameters gives the theoretical upper bound for the storage capacity per spatial location as a result of the presence of the wavelength dimension. This material has two optically equivalent sites for the transition; the other site (Site 2)

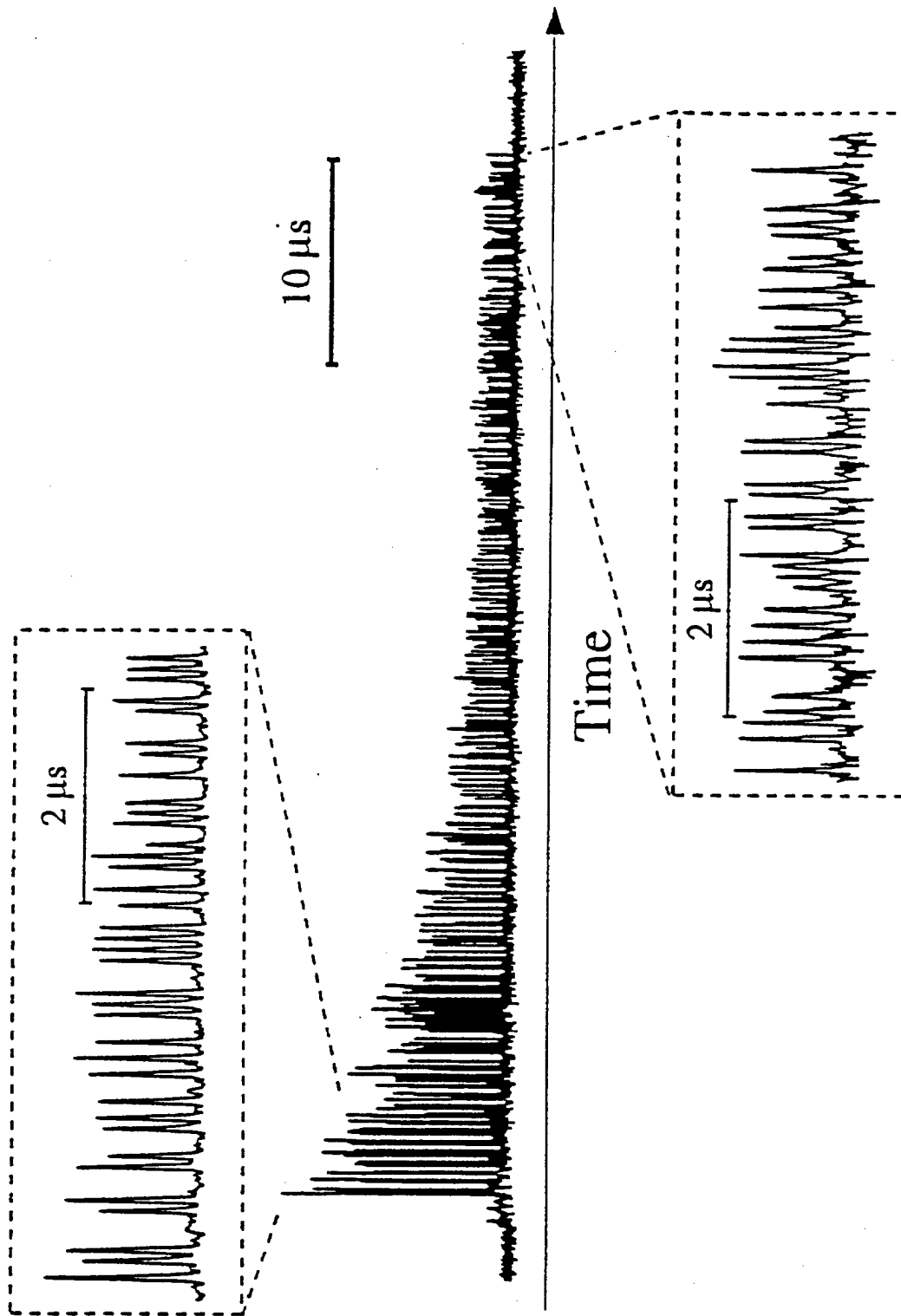


Figure 5. Storage of 1020 bits of data. The string is the ASCII representation of "Time-Domain Holography, Dynamic Optical Memory, Reprogrammable Optical Delay Lines at 1.5 microns" encoded with the (1.7) code. An exponential intensity ramp is used to compensate to the large decrease of the intensity of the retrieved data over 50 μs. The peak power is measured to be ~0.25 μW. All of the data traces shown in this figure represent single recording and retrieval events and are detected by an avalanche photodiode module with a gain of 9.4 V/μW at 1.55 μm.



has a comparable linewidth and dephasing time, making the material a good candidate for high capacity applications. During the experiments, the crystal was kept at a temperature of about 4 K in a flowing He-vapor cryostat.

Each data page is stored in a distinct, narrow (~500 kHz) frequency channel within the inhomogeneously broadened absorption line by wavelength division multiplexing (WDM). The separation between two adjacent channels is chosen to be approximately 800 kHz. WDM has several distinct advantages. Recording and retrieval can be accomplished without use of any moving parts for laser beam steering. Therefore, it is inherently reliable and often provides short access times. In addition, WDM is expected to have no significant effect on diffraction efficiency. Each data page can be recorded in an identical manner, no scheduled recording or incremental recording as used in angular division multiplexing [14] are needed, increasing considerably the recording speed.

The spatial light modulator used in the present experiment to generate two dimensional digital data is a liquid crystal array taken from a commercial projection television. The array consists of  $480 \times 440$  pixels and has a low fill factor of ~24%. This low fill factor introduces a large insertion loss in the transmitted beam. We measured the loss for the zeroth-order transmission to be ~97% at 580 nm.

The retrieved data was captured by an intensified CCD camera which has an array of  $768 \times 484$  pixels. The captured images were further digitized at reduced horizontal resolution of 640 pixels per line by a frame grabber. The mismatch between the CCD and SLM, and that between the frame grabber and CCD, as well as the low spatial resolution of the intensifier (~64 lp/mm), prevented the use of small bit dimensions in our experiment. We chose  $5 \times 5$  pixels on the SLM to represent a data bit and used a total of 3360 bits ( $60 \times 56$  bits) in each data frame to cover a center area equal to approximately 40% ( $\sim 1.6 \times 1.3 \text{ cm}^2$ ) of the SLM. The data frame was imaged (1:1) on to the CCD array, resulting in an average bit size of  $10.7 \times 8.4$  pixels after digitization. We used these mismatched devices because they were readily available at the time of the experiments, and no attempt was made to match the dimensions of the devices. Obviously, choosing matched SLM, CCD and frame grabber would allow the use more data bits per frame, which would increase the storage capacity as well as the data transfer rate.

The write/read pulses used in the present experiment were 10  $\mu\text{s}$  long square pulses with a peak power of ~200 mW only. These pulses were biphase-encoded with the 5-bit Barker code [15] to increase data channel width to ~500 kHz. The reason for introducing this modulation is to make our system more tolerant to laser wavelength instability and hence reduce the fluctuation of echo intensity. The length of the data pulse used in our experiment varied from 11.2 to 50  $\mu\text{s}$ . This data pulse was also biphase modulated by using pseudorandom code [16] to further reduce the echo fluctuation caused by laser wavelength instability.

Both the SLM and CCD operated at the maximum video rate (i.e., 30 frames per second) and the resulting digitized data was stored in the dynamic memory of a computer at the same

speed. Compared to 11.6  $\mu$ s per page exposure time used in our experiment, this video rate obviously limits the sustainable I/O speed of our system substantially. This limit however is not fundamental and can be increased to match the speed set by the exposure time.

**Analysis of page-formatted binary data.** In digital memories, one important parameter determining the memory's performance is the bit error rate (BER), which measures how often an error bit would occur on average. This parameter is closely related to other performance parameters of the system, such as storage capacity, data transfer rates and data access times. For a given system in general, attempting to reduce the BER often leads to a decrease of storage capacity and/or data transfer rate, because a low BER requires high signal-to-noise ratios. For parallel recording, it means the need of a large modulation transfer function which implies the use of large bit dimensions. For a fixed frame size, for example, it translates into a decrease of the data transfer rate.

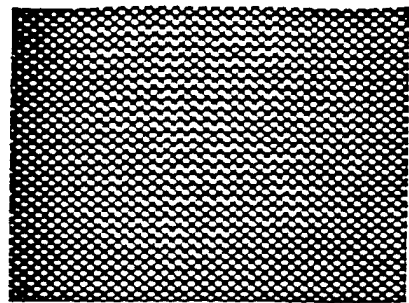
For an optical storage system operating at high I/O speeds with low laser power illumination, the retrieved data are often at a signal level close to shot noise limited. For page-formatted recording, it is further complicated by the nonuniform illumination of a SLM. Because of these undesired conditions associated with low photon budget, such a system often experiences large page-to-page fluctuations and intra-page variations.

Figure 6a shows a sample input page used in data recording. Here, spatial variation of intensity is apparent. This variation reflects the spatial beam mode of the addressing laser, contributing partially to the spatial signal variations within a page discussed earlier. The other contributions include shot noise resulting from the quantum nature of photons.

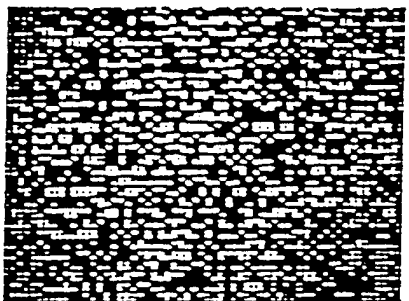
The page-to-page fluctuation is often more noticeable in the retrieved data because it is magnified by less than ideal recording and readout conditions. Figures 6b and 6c show two retrieved pages that represent the brightest and dimmest among a total of 100 pages recorded in an experiment. They are single readout events with no signal averaging. The intensity difference between the two pages is >300%.

Further examining the histogram of all 100 pages (totaling 336 kbits of data), we found that the intensity distributions of the 1's (or ON's) and 0's (or OFF's) partially overlap as shown in Figure 7. If a single threshold were used to determine all the data bits, it would lead to a BER as large as  $10^{-3}$ , not suitable for any storage application.

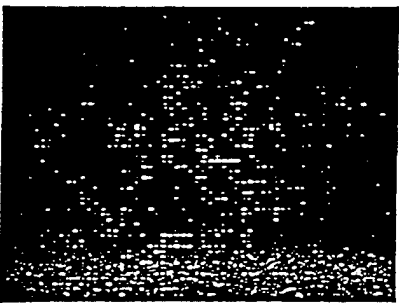
We use recently determined data bits to obtain a local threshold for the next bit under consideration. The local region is chosen in such a way it occupies an area that is small enough so that the illumination is approximately uniform, yet large enough to have a sufficient number of bits for an adequate average. Under such a condition, a threshold can be derived from the



(a)



(b)



(c)



(d)

Figure 6. (a) Input data image after transmitted through the  $\text{Eu}^{3+}:\text{Y}_2\text{SiO}_5$  sample. (b) Reconstructed image after being stored in  $\text{Eu}^{3+}:\text{Y}_2\text{SiO}_5$  for 200  $\mu\text{s}$ . (c) Image reconstructed under the same condition as that of (b) but with weak overall intensity. (d) Image reconstructed 5 minutes after the completion of recording. In (a)-(c), the data pulse length was 11.6  $\mu\text{s}$ , and that in (d) was 50  $\mu\text{s}$ . The former corresponds to an I/O rate of 300 megabits per second while the latter corresponds to 67 megabits per second.

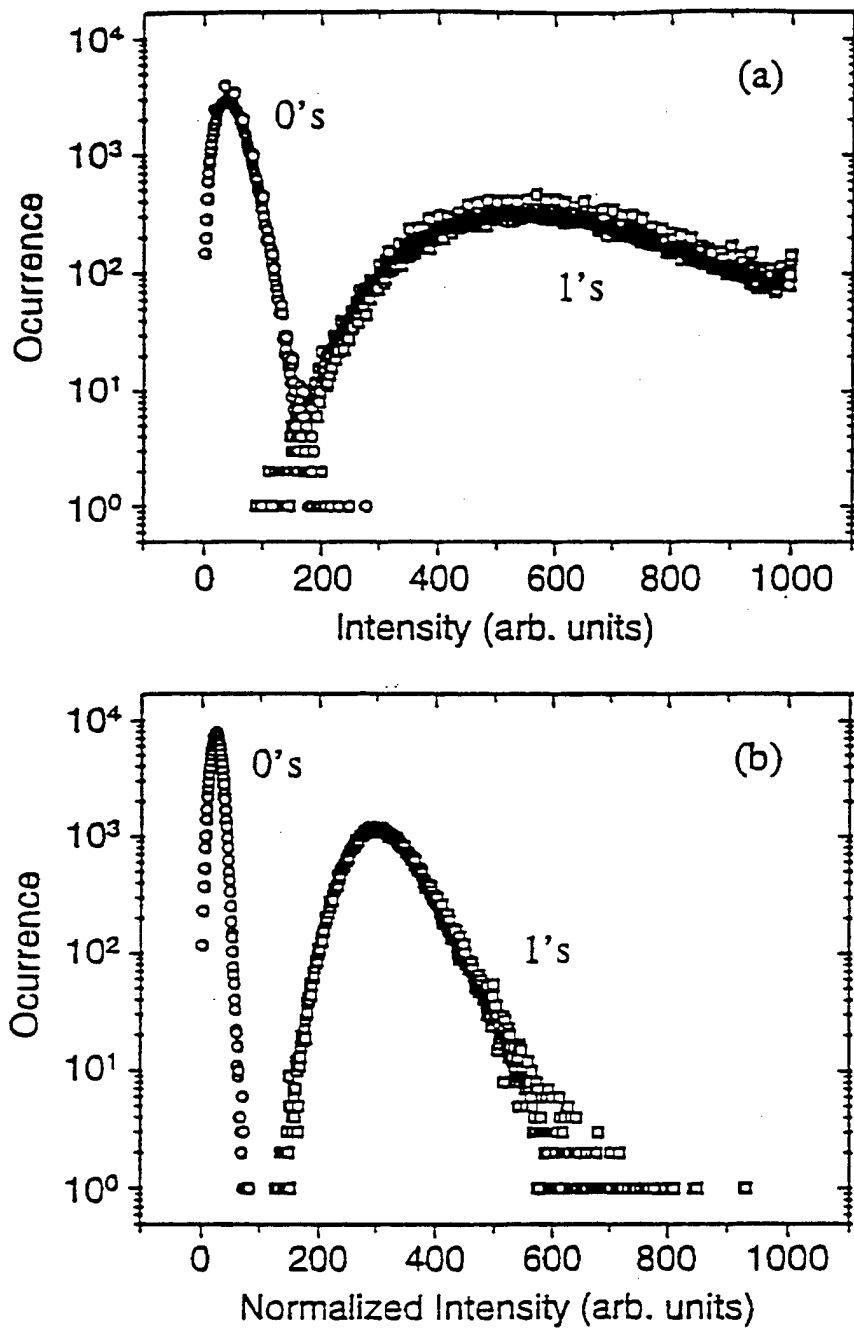


Figure 7. (a) Histogram showing the intensity distributions of 0's and 1's that were retrieved from the time-domain memory. (b) Normalized histogram obtained after applying the local threshold technique.

Poisson distributions to accurately determine the state of the bit, provided that the intensity within a page varies smoothly. We adopted the following formula for the threshold

$$I_{thr} = I_0 + p\sqrt{I_0} + q[(I_1 - p\sqrt{I_1}) - (I_0 + p\sqrt{I_0})]$$

where  $I_0$  and  $I_1$  are the averages of 0's and 1's,  $q$  is a weighting factor chosen empirically to be 1/3, and  $p$  is a measure of how many standard deviations above  $I_0$  and below  $I_1$  we can place the threshold. Here, we use  $p=11$ . The optimum numbers used in averaging were found to be four for 0's and eight for 1's.

Obviously, we need to provide initial  $I_0$  and  $I_1$  to jump start the analysis of each page. This is accomplished by placing 4 known 0-bits permanently at the corners of a 4x4 region in the center of the SLM where the signal-to-noise rate is largest. We average the 4 bits to estimate  $I_0$ . A crude estimate for  $I_1$  can be obtained by averaging the intensities of the remaining twelve unknown bits. The threshold for the block is then calculated from the above equation by assuming the block intensity  $I_{blk} = (I_0 + I_1)/2$  which implies an equal number of 1's and 0's in the block. This approach yields a BER of  $10^{-6}$  for the 12-bit central region, or equivalently a  $10^{-5}$  probability of having an error bit per page.

We then continue this analysis process by spiraling outward from the center of a page towards the edges with the intensity decreasing gradually as the analysis proceeds. The neighboring 1's and 0's are stored in two separate register arrays and updated in a first-in-first-out manner to obtain their running averages. Thus, each data bit is determined in real time with the use of the equation above. In comparison to the existing schemes for reading page-formatted digital data [14], this automatic threshold calibration technique uses no coding bits and requires no mathematical iteration. These advantages lead to a significant increase in the readout rate, ideal for high-speed applications.

**System performance and projections.** Using this new approach, we repeated the above experiment and obtained a histogram for the same 100 pages used earlier (Figure 7b). This histogram was normalized to the respective threshold of each data bit and it shows two clearly separate distribution curves. The separation is found to be approximately 40% of the full width of the distribution for 0's. This large separation suggests an effective increase of the system's dynamic range by ~40%. The raw BER is estimated to be  $\sim 10^{-7}$ . We further verified this number by repeating the experiment over 10 times and found that the two distribution curves in the resulting histogram remain separate.

In obtaining the above results, we chose the data pulse to be 11.2  $\mu$ s long, which translates to an I/O rate of 300 megabits per second. The 100 pages were wavelength-division multiplexed at a single storage cell approximately 1.0 mm  $\times$  1.0 mm  $\times$  7.0 mm at a rate of 30 frames per second with a total recording time of ~3.3 seconds. All the pages used in the

histogram were obtained from the same experiment. For convenience, each data page used for BER analysis was retrieved after being transferred to the memory for 200  $\mu$ s. Using short storage time prevents undesired page-to-page fluctuation caused by slow frequency drift of our laser. The echo (or "diffraction") efficiency for the short term storage was measured to be  $\sim 5 \times 10^{-3}$ .

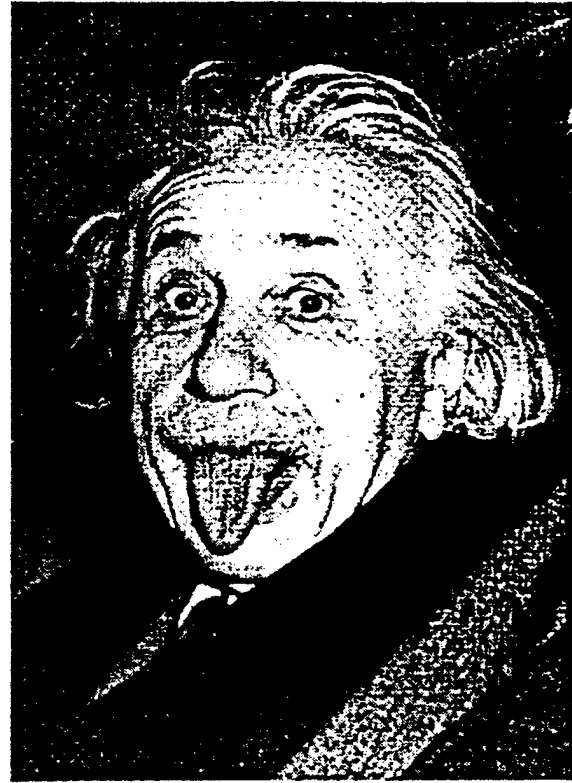
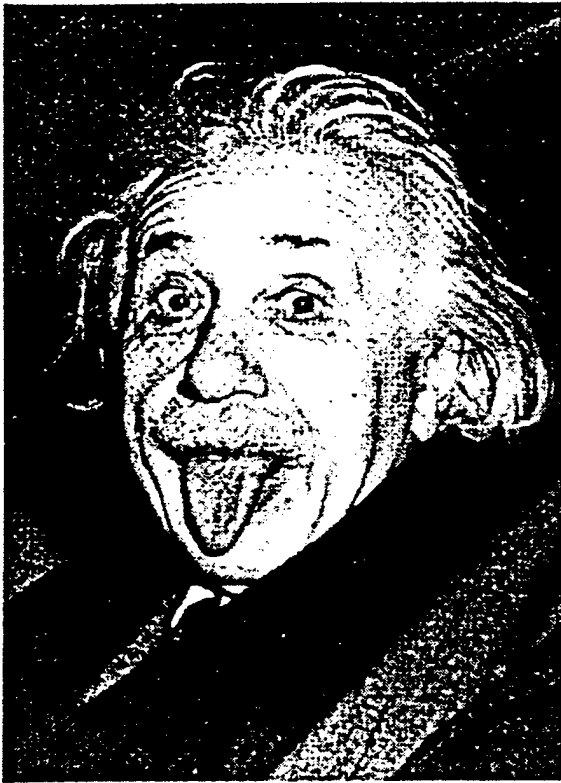
According to our BER measurement, our current storage system is capable of recording digital data close to 10 megabits without generating an error bit. To demonstrate it, we performed an experiment in which we stored a high resolution black-white photograph of Albert Einstein (Figure 8a). This digitized photograph contains 106 pages totaling 356 kbits of digital data. Figure 8b shows the reconstructed photograph after being copied to and read back from the memory. The entire photograph was stored at a single spatial location in  $\text{Eu}^{3+}:\text{Y}_2\text{SiO}_5$  using WDM with a peak recording speed of 300 megabits per second and no error correcting code of any kind was used. The total material bandwidth used was only  $\sim 85$  MHz.

The present work represents the first experimental demonstration of parallel digital data storage utilizing the time-domain approach. It opens up the possibility of developing the technology into a high-performance page-oriented dynamic optical memory. As the technology for parallel data access becomes more mature, this time-domain holographic approach along with other optical holographic storage techniques (e.g., the photorefractive memory) may be able to fulfill their long awaited promise for high-speed high-density data storage.

However, a number of issues need to be addressed before this technology can be considered commercially viable. One of them is the low operating temperature currently required. We hope that the present work will generate sufficient interests in the scientific community so that these important but difficult issues can be addressed and hopefully resolved promptly.

Original

Reconstructed



(a)

(b)

Figure 8. (a) Digitized photograph displayed using its original binary data. (b) Same photograph obtained after the binary data being transferred to and then recalled back from the time-domain memory.

## CONCLUSIONS AND RECOMMENDATION

In conclusion, we have demonstrated the practical viability of the stimulated echo approach using rare-earth doped material to buffer optical data. This was demonstrated in bit serial and bit parallel approach. In addition, we have identified new materials which allow the storage of data in the 1.5  $\mu\text{m}$  optical range. Optical switching of data packets in the next generation optical networks is therefore feasible.



## REFERENCES

1. T. W. Mossberg, *Opt. Lett.* **7**, 77 (1982).
2. Y. S. Bai and R. Kachru, U.S. Patent 5,369,665 (November 29, 1994).
3. M. Mitsunaga, R. Yano, and N. Uesugi, *Opt. Lett.* **16**, 1890 (1991).
4. X. A. Shen, E. Chiang, and R. Kachru, *Opt. Lett.* **19**, 1246 (1994).
5. H. Lin, T. Wang, and T. W. Mossberg, *Opt. Lett.* **20**, 1658 (1995).
6. Y. S. Bai, W. R. Babbitt, N. W. Carlson, and T. W. Mossberg, *Appl. Phys. Lett.* **45**, 714 (1984).
7. X. A. Shen, Y. S. Bai, and R. Kachru, *Opt. Lett.* **17**, 1079 (1992).
8. M. Zhu, C. M. Jefferson, and W. R. Babbitt, in *Spectral Hole-Burning and Related Spectroscopies: Science and Applications*, Vol. 15, 1994 OSA Technical Digest Series (Optical Society of America, Washington, DC 1994), p. 392.
9. M. K. Ashurov, Y. K. Voronko, V. V. Osiko, A. A. Sobol, B. P. Starikov, M. I. Timoshechkin, and A. Y. Yablonskii, *Phys. Stat. Sol. (a)* **35**, 645 (1976).
10. J. A. Koningstein and J. E. Geusic, *Phys. Rev.* **136**, A726 (1964).
11. T. W. Mossberg, R. Kachru, S. R. Hartmann, and A. M. Flusberg, *Phys. Rev.* **A20**, 1976 (1979).
12. Y. Zhang and R. Kachru, *Appl. Opt.* **35**, 6762 (1996).
13. R. M. Macfarlane and R. M. Shelby, *Opt. Comm.* **42**, 346 (1982).
14. J. F. Heanue, M. C. Bashaw, and L. Hesselink, *Science* **265**, 749 (1994).
15. See, for example, M. N. Cohen, in *Principles of Modern Radar*, J. L. Eaves and E. K. Reedy, eds. (Van Nostrand Reinhold, New York, 1987), p. 465.
16. Y. S. Bai and R. Kachru, *Opt. Lett.* **18**, 1189 (1993).

**APPENDIX A**

**OPTIMIZATION OF TIME-DOMAIN STORAGE DENSITY IN THE  
PRESENCE OF EXCITATION-INDUCED SPECTRAL DIFFUSION**

# Optimization of time-domain storage density in the presence of excitation-induced spectral diffusion

X. A. Shen and R. Kachru

We present a technique to reduce the loss of storage capacity in time-domain optical memory in the presence of excitation-induced spectral diffusion. We applied this technique to a  $\text{Eu}^{3+}:\text{Y}_2\text{SiO}_5$ -based memory that utilizes frequency chirp for recording-retrieval and successfully stored 860 bits of data in a 40-MHz data channel. In comparison with the conventional chirp method under identical experimental conditions, the present technique offers an increase of a factor of  $\sim 2$  in storage capacity with no measurable loss of signal fidelity. The results are interpreted in terms of the phase error accumulated during dephasing-rephasing and spectral diffusion on excited-state relaxation. © 1997 Optical Society of America

*Key words:* Time-domain optical memory, photon echoes, frequency chirp, excitation-induced spectral diffusion.

Since proposed in the early 1980's,<sup>1</sup> coherent time-domain optical memory (TDOM) has emerged as a strong candidate for next-generation storage devices. In TDOM, data can be stored and recalled rapidly in either bit-serial or bit-parallel formats, providing unprecedented flexibility for diversified applications varying from optical packet switching to high-speed image processing. Single-channel storage-retrieval of serial data at 40 Mbits/s, parallel recording at an input-output speed of  $\sim 20 \mu\text{s}/\text{frame}$ , as well as a storage density of  $\sim 8 \text{ Gbits}/\text{in.}^2$  ( $\sim 8 \text{ Gbits}/6.45 \text{ cm}^2$ ) have been demonstrated with cw lasers of a modest peak power.<sup>2-4</sup>

While the theoretical limits of the bandwidth and storage capacity are substantially high for TDOM as a result of the presence of the frequency dimension for recording (typically 5–10 GHz and  $10^6$ – $10^7$  bits/focal volume for rare-earth-doped solids), reaching these limits remains a challenge. One of the obstacles is the presence of excitation-induced spectral diffusion (EISD)<sup>5-9</sup> that results from interactions among

active ions during information recording-retrieval. This process leads to a broadening of the recorded spectral gratings, which in turn reduces the useable storage capacity of the memory.

Here we present a technique to maximize the storage capacity of TDOM in the presence of EISD. We choose frequency-chirp recording as an example and show that, with the proposed technique, an increase of a factor of  $\sim 2$  in the storage density can be achieved in a  $\text{Eu}^{3+}:\text{Y}_2\text{SiO}_5$ -based memory.

In TDOM, information is stored in a recording medium by a write pulse  $E_W$ , which often precedes the data pulse by a time  $\tau$  and serves as a temporal reference for data retrieval. To retrieve the information  $T$  (storage time) after the arrival of the data pulse, the recording medium is reexposed to a read pulse  $E_R$ , which induces coherent radiation  $E_E$  known as stimulated-photon echo.  $E_E$  occurs also at a time  $\tau$  after the arrival of  $E_R$  and is related to the three inputs as follows:

$$\vec{E}_E(\nu) \propto \vec{E}_W^*(\nu) \vec{E}_R(\nu) \vec{E}_D(\nu), \quad (1)$$

where  $\vec{E}_i$  is the Fourier transform of  $E_i$ .

In TDOM, EISD manifests itself as a loss of echo intensity, but in two distinct manners<sup>6,9</sup>: a rapid decrease of instantaneous echo power as  $\tau$  increases, and a decrease of overall echo intensity as  $T$  increases. The former is known as excitation-induced excess dephasing, which is found to result from phase

The authors are with the Molecular Physics Laboratory, SRI International, 333 Ravenswood Avenue, Menlo Park, California 94025.

Received 14 October 1996; revised manuscript received 18 March 1997.

0003-6935/97/266692-04\$10.00/0

© 1997 Optical Society of America

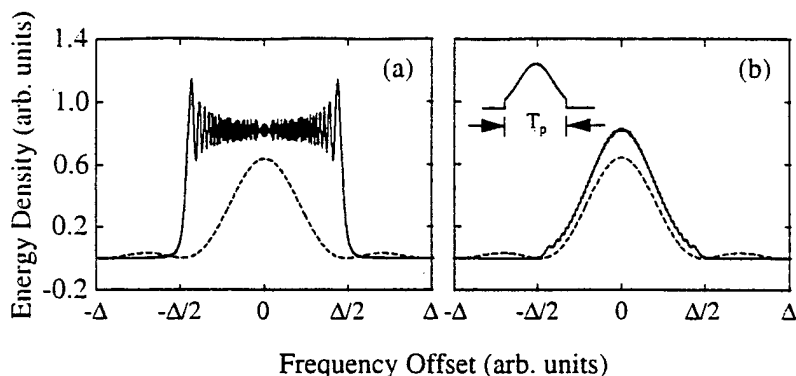


Fig. 1. (a) Power spectrum of a linearly chirped pulse with a rectangular envelope (solid curve) and (b) the power spectrum of an identically chirped pulse (solid curve) with a truncated Gaussian envelope (the insert). Here,  $\Delta$  is the chirp width and  $T_p\Delta = 256$ . The dashed curves in both (a) and (b) are the same spectrum of a brief rectangular pulse of length  $\tau = 2/\Delta$ .

errors accumulated by active ions during data recording ( $0 \rightarrow \tau$ , dephasing time) and retrieval ( $T + \tau \rightarrow T + 2\tau$ , rephasing time).<sup>6-10</sup> These errors are generated by interaction with neighboring ions undergoing a change of electronic states on laser excitation. These ions modify the electric field seen by an active ion, giving rise to a shift of its transition frequency. The larger the time  $\tau$ , the higher the probability for this ion to accumulate a phase error.

When  $\tau \rightarrow 0$ , excess dephasing vanishes, and spectral diffusion becomes dominant. Depending on the choice of  $T$ , a number of diffusion mechanisms may be present.<sup>11,12</sup> For values of  $T$  comparable with the excited-state lifetime  $T_1$ , diffusion from excited-state ion relaxation often dominates. This process results in a broadening of the spectral grating generated by  $E_W$  and  $E_D$ , which leads to a loss of echo intensity, hence a loss of storage capacity.

EISD is determined by the concentration of excited-state ions. For a spectrally and spatially uniform ion distribution, EISD is then determined by the energy of the excitation pulses. The lower the pulse energy, the weaker the EISD. Thus, preventing EISD-mediated memory-capacity loss reduces to finding laser pulses that offer a maximum  $E_E$  at a fixed pulse energy.

For convenience, we assume the following: (a) The data stream to be stored consists of only one short rectangular pulse  $E_D$  of a length  $\tau$  and an amplitude  $E_{D0}$ , and (b)  $E_W = E_R$ . To make our analysis independent of EISD, we compare different recording methods under identical energies for  $E_W$  and  $E_R$ .

We first examine the conventional chirp method<sup>13,14</sup> for which we obtain  $E_W$  and  $E_R$  by linearly sweeping the carrier frequency of a fixed-power laser pulse. Figure 1(a) shows the power spectrum (the solid curve) of such a pulse with  $\Delta T_p = 256$ , where  $\Delta$  is the chirp width and  $T_p$  is the pulse length. The dashed curve in Fig. 1(a) is the power spectrum of the data pulse defined above. We chose  $\Delta \sim 2/\tau$  (the full width of the data pulse at the first minima). For minimizing the EISD,  $\Delta$  must be equal to  $\sim 2/\tau$  because at a given chirp rate a larger  $\Delta$  means more energy is deposited outside of the data bandwidth,

and those energies contribute only weakly to  $E_E$  but equally to EISD.

Even under the condition of  $\Delta = 2/\tau$ , the conventional chirp method deposits an equal amount of energy at the band edges, where the data signal nearly vanishes [see Fig. 1(a)]. This implies that the conventional method does not use the energy of  $E_W$  and  $E_R$  efficiently. If EISD were present, it would certainly result in a small echo signal and consequently a low storage density.

One approach that utilizes the pulse energy efficiently is to chirp  $E_W$  and  $E_R$  in such a way that their power spectra resemble closely that of the data pulse. Since the desired spectra are identical to that of the data pulse, we can estimate  $E_E$  generated by such chirped pulses by using simple, brief  $E_W$  and  $E_R$  pulses that are temporally identical to  $E_D$ . For a brief  $E_W (=E_R)$  of a length  $\tau$  and amplitude  $E_0$ , the resulting peak-echo amplitude  $E_{E0}^{\text{brief}} \propto 3E_0^2 E_{D0} \tau^2 / 4$  with a full width at half-maximum of  $\sim 1.26\tau$ .

We can compare the above amplitude to that obtained with the conventional chirp method. Notice that, for a rectangular chirped  $E_W$  (here  $\Delta = 2/\tau$ ) to have the same energy as the above brief pulses, its spectrum peak  $|\bar{E}_W|_{\text{max}}^2$  must satisfy  $|\bar{E}_W|_{\text{max}}^2 \Delta \approx E_0^2 \tau$ . From relation (1) we obtain a peak-echo amplitude  $E_{E0}^{\text{rect}} \propto E_0^2 E_{D0} \tau^2 / 2$ , with a width of  $\sim \tau$ , where the superscript rect denotes rectangular. Therefore, we have a ratio of  $E_{E0}^{\text{brief}} / E_{E0}^{\text{rect}} \approx 3/2$  and a corresponding intensity ratio of  $\sim 9/4$ .

The above analysis states that, in the presence of EISD, an increase of a factor of  $\sim 2.25$  in the echo power can be achieved by redistribution of the energy of  $E_W$  and  $E_R$  in such a way that their power spectra are identical to that of the data pulse to be stored. In TDOM's utilizing frequency chirp for recording-retrieval, this can be accomplished by appropriate modulation of the amplitudes of  $E_W$  and  $E_R$  so that the energy at the band edges (which corresponds to the early and later parts of  $E_W$  and  $E_R$ ) is reduced.

Figure 1(b) shows the power spectrum obtained by replacement of the conventional chirped pulse [Fig. 1(a)] with a chirped pulse whose envelope resembles

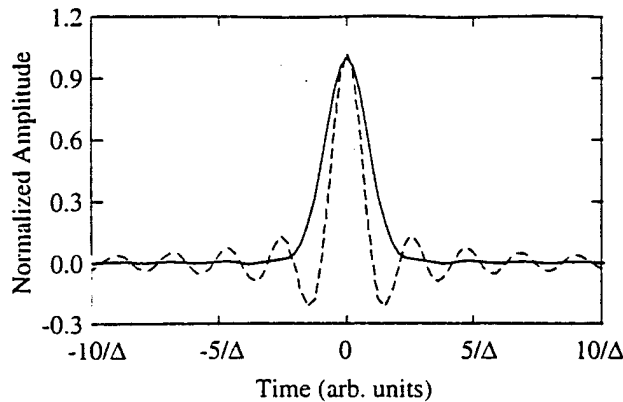


Fig. 2. Autocorrelations of the same pulses shown in Figs. 1(a) (dashed curve) and 1(b) (solid curve). Here,  $\Delta$  is the chirp width.

a truncated Gaussian curve of the same length [Fig. 1(b)]. Here, the Gaussian width (full width at  $1/e$ ) was chosen to be  $\sim 0.78T_p$ . Calculations show that the echo intensity obtained with such pulses is higher by a factor of  $\sim 2.0$  than that obtained with conventional chirped pulses of the same energy and that the width of the retrieved pulse is  $\sim 1.26\tau$ , which is in good agreement with the estimates obtained with brief  $E_W$  and  $E_R$  pulses.

In digital data storage, the broadening of a subpulse in a data stream leads to an increase of the signal level between two adjacent pulses. If the peak of a subpulse represents 1 and the absence of a pulse represents 0, this broadening translates to a broadening of the intensity distribution of 0's. Careful examination of  $F^{-1}\{\tilde{E}_W^*(\nu)\tilde{E}_R(\nu)\}$  (the inverse Fourier transform representing the correlation of  $E_R$  with  $E_W$ ) for the above two methods shows that the conventional chirp, although it offers a sharper correlation peak, generates large sidelobes (the dashed curve in Fig. 2), which cause a fluctuation of the echo amplitude and consequently a broadening of the distribution of 1's. The proposed chirp method, on the other hand, has a broadened correlation peak but negligible sidelobes (the solid curve in Fig. 2), the latter reducing the intensity fluctuation of 1's. Calculations show that the sum of the two distribution widths (a measure of the system's bit-error rate) is actually reduced by  $\sim 27\%$  with the use of the proposed method.

In the implementation of TDOM,  $E_W$  and  $E_R$  are often obtained by modulation of a cw laser externally.<sup>2-4</sup> The maximum achievable peak power is thus fixed. We have shown that, if EISD were present, using the conventional chirp method with a reduced peak power would result in a loss of a factor of  $\sim 2$  in the signal intensity, which in turn leads to a loss of storage capacity. The only question that remains to be answered is which of the two chirp methods would offer a higher storage density if both were operated at the same peak power. Obviously, the conventional method would give a larger echo signal if EISD were absent because more energy would be used. If EISD were present, the answer

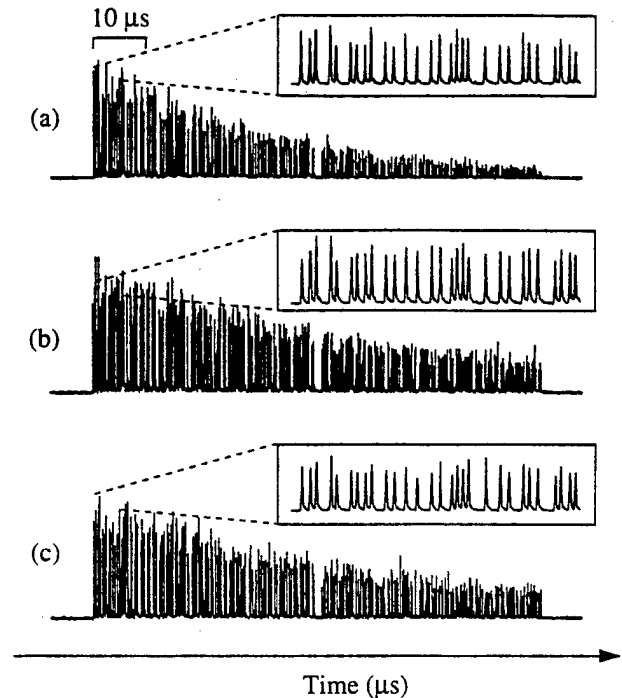


Fig. 3. Data retrieved from a  $\text{Eu}^{3+}:\text{Y}_2\text{SiO}_5$ -based memory by use of three different pairs of  $E_W$  and  $E_R$ : (a) linearly chirped  $E_W$  and  $E_R$  with a rectangular envelope, (b) identically chirped  $E_W$  and  $E_R$  with a truncated Gaussian envelope (full width at  $1/e = 0.78T_p$ ), and (c) identically chirped  $E_W$  and  $E_R$  with an envelope corresponding to the first half of a sine function. In all three cases, the peak laser power,  $T_p$ , and  $\Delta$  remain the same, and they are  $\sim 100$  mW,  $6.4$   $\mu\text{s}$ , and  $40$  MHz, respectively.

would depend on the storage material and would have to be determined experimentally.

We performed an experiment on the  ${}^7F_0$ - ${}^5D_0$  transition in  $\text{Eu}^{3+}:\text{Y}_2\text{SiO}_5$  to address this question. We chose  $\text{Eu}^{3+}:\text{Y}_2\text{SiO}_5$  because in this material diffusions other than EISD were found to be insignificant below  $4$  K,<sup>8</sup> and any loss of echo intensity could be attributed primarily to EISD. The experimental apparatus and conditions were identical to those described in Ref. 15.

We stored identical data streams that contain 860 bits of data using three different chirp methods: (a) the conventional chirp method, (b) chirped  $E_W$  and  $E_R$  with the truncated Gaussian amplitude envelope discussed above, and (c) chirped  $E_W$  and  $E_R$  with an envelope equal to the first half of the sine function. In all three cases, the peak power of  $E_W$  and  $E_R$ ,  $T_p$ ,  $\Delta$ , the laser beam waist, the separation between  $E_W$  and  $E_D$ , and the separation between  $E_D$  and  $E_R$  are chosen to be identical, and they are, respectively,  $\sim 100$  mW,  $6.4$   $\mu\text{s}$ ,  $40$  MHz,  $\sim 100$   $\mu\text{m}$  (FWFM),  $18$   $\mu\text{s}$ , and  $240$   $\mu\text{s}$ . The length of each data subpulse was  $\sim 50$  ns, giving rise to a data length of  $\sim 90$   $\mu\text{s}$  and a bandwidth equal to  $\Delta$ . The pulse energy used in method (a) was  $\sim 2.1$  times larger than that of methods (b) and (c).

Figures 3(a)-3(c) show the experimental results obtained with the above three methods, respectively.

The peak-echo powers in all three cases are nearly identical. The conventional chirp method (a) yields a faster decay in comparison with the other methods, which show decay rates comparable with each other. If the signals at the ends of the data strings shown in Figs. 3(b) and 3(c) correspond to the minimum resolvable signal level of our system, then the fast signal decay shown in Fig. 3(a) translates to a loss of a factor of  $\sim 2$  in data capacity. The exact gain of the storage capacity requires careful examination of the fidelity of each data bit. However, visual inspection of the echo data shows no apparent degradation of signal fidelity with the use of the proposed technique (see the inserts in Figs. 3).

Plotting the results on a logarithmic scale shows that the decays closely follow the function  $\exp(-\Gamma_{\text{ex}}t)$ , with  $\Gamma_{\text{ex}} \sim 1/(33 \mu\text{s})$  for Fig. 3(a) and  $\Gamma_{\text{ex}} \sim 1/(65 \mu\text{s})$  for Figs. 3(b) and 3(c). Extrapolation of the data to the center of the read pulse (i.e.,  $\tau \rightarrow 0$ ) yields an echo-intensity ratio between the results of Figs. 3(a) and 3(b) [or Figs. 3(a) and 3(c)] of  $\sim 1.2$ , much smaller than the value of 2.2 calculated in the absence of EISD. This difference can be attributed to partial relaxation of the excited-state ions generated by the additional ( $\sim 51\%$ ) pulse energy used in the conventional chirp method. The ratio between the two decay constants [i.e.,  $(65 \mu\text{s})/(33 \mu\text{s}) = 1.97$ ] is a direct measure of the gain in storage capacity obtained with the proposed technique.

In conclusion, we have presented a novel technique to increase the useable storage capacity of a TDOM in the presence of EISD. This technique has been tested experimentally in  $\text{Eu}^{3+}:\text{Y}_2\text{SiO}_5$  and an increase of a factor of  $\sim 2$  in storage capacity has been achieved.

We express our appreciation to John W. Perry for the numerical simulation. This research was supported by the Defense Advanced Research Projects Agency under contract F-49620-95-C-0077.

#### References and Notes

1. T. W. Mossberg, "Time-domain frequency-selective optical data storage," *Opt. Lett.* **7**, 77-79 (1982).

2. Y. S. Bai and R. Kachru, "Coherent time-domain data storage with a spread spectrum generated by random biphasic shifting," *Opt. Lett.* **18**, 1189-1191 (1994).
3. X. A. Shen, E. Chiang, and R. Kachru, "Time-domain holographic image storage," *Opt. Lett.* **19**, 1246-1248 (1994).
4. H. Lin, T. Wang, and T. W. Mossberg, "Demonstration of 8 Gbit/in.<sup>2</sup> areal storage density using swept-carrier frequency-selective optical memory," *Opt. Lett.* **20**, 1658-1660 (1995).
5. J. Huang, J. M. Zhang, A. Lezama, and T. M. Mossberg, "Excess dephasing in photon-echo experiments arising from excitation-induced electronic level shifts," *Phys. Rev. Lett.* **63**, 78-81 (1989).
6. M. Mitsunaga, T. Takagahara, R. Yano, and N. Uesugi, "Excitation-induced frequency shift probed by stimulated photon echoes," *Phys. Rev. Lett.* **68**, 3216-3219 (1992).
7. Y. S. Bai and R. Kachru, "Nonequilibrium resonant-phonon-induced excess photon-echo dephasing," *Phys. Rev. B* **46**, 13,735-13,738 (1992).
8. R. W. Equall, T. Sun, R. L. Cone, and R. M. Macfarlane, "Ultralow optical dephasing in  $\text{Eu}^{3+}:\text{Y}_2\text{SiO}_5$ ," *Phys. Rev. Lett.* **72**, 2179-2182 (1994).
9. Y. S. Bai and M. D. Fayer, "Time scales and optical dephasing measurements: investigation of dynamics in complex systems," *Phys. Rev. B* **39**, 11,066-11,084 (1989).
10. J. R. Klauder and P. W. Anderson, "Spectral diffusion in spin resonance experiments," *Phys. Rev.* **125**, 912-932 (1962).
11. W. B. Mims, "Phase memory in electron spin echoes, lattice relaxation effects in  $\text{CaWO}_4:\text{Er, Ce, Mn}$ ," *Phys. Rev.* **168**, 370-389 (1968).
12. R. M. Macfarlane and R. M. Shelby, "Coherent transient and holeburning spectroscopy of rare earth ions in solids," in *Spectroscopy of Solids Containing Rare Earth Ions*, A. A. Kaplyankii and R. M. Macfarlane, eds. (North-Holland, Amsterdam, 1987), pp. 51-184 and references therein.
13. Y. S. Bai, W. R. Babbitt, and T. W. Mossberg, "Coherent transient optical pulse-shape storage-recall using frequency-swept excitation pulses," *Opt. Lett.* **11**, 724-726 (1986).
14. S. Kröll, L. E. Jusinski, and R. Kachru, "Frequency-chirped copropagating multiple-bit stimulated-echo storage and retrieval in  $\text{Pr}^{3+}:\text{YAlO}_3$ ," *Opt. Lett.* **16**, 517-519 (1991).
15. X. A. Shen and R. Kachru, "Experimental demonstration of impulse-equivalent time-domain optical memory," *Opt. Lett.* **21**, 2020-2022 (1996).

**APPENDIX B**

**OBSERVATION OF PHOTON ECHO IN ER<sup>3+</sup>:YAG AT 1.527  $\mu\text{m}$**

# Observation of photon echo in $\text{Er}^{3+}:\text{YAG}$ at $1.527 \mu\text{m}$

Y. Zhang, X. A. Shen, and R. Kachru

Molecular Physics Laboratory, SRI International, Menlo Park, California 94025

Received January 24, 1997

We report what is to our knowledge the first experimental observation of two- and three-pulse echoes in  $\text{Er}^{3+}:\text{YAG}$  at  $1.527 \mu\text{m}$ . The experiment was performed on the transition from the  $^4I_{15/2}$  ground state to the lowest Stark level of the  $^4I_{13/2}$  excited state. The corresponding homogeneous dephasing time was measured to be approximately 50 ns at 1 and 7 K. In addition, three-pulse echo decay indicated a lifetime of the spectral grating of  $\sim 30 \mu\text{s}$ . Implications of these results for optical data storage and optical signal processing are discussed. © 1997 Optical Society of America

Photon echo in solids provides not only important spectroscopic information about the dynamic interactions among active ions and their host materials but also a powerful means of storing and processing temporal signals of various kinds at optical wavelengths; the latter feature led to the proposal and successful experimental demonstration of coherent time-domain optical memory (TDOM).<sup>1-5</sup> Unlike other optical memories, TDOM is a high-speed signal processor by nature. Temporal data strings stored at different times can be correlated or convoluted simultaneously with an incoming data string in the memory at bandwidths of up to several gigahertz, with no additional processing time required.<sup>6-8</sup> This rapid in-memory processing feature combined with the demonstrated high storage capacity also makes TDOM a superior candidate for applications such as high-speed optical packet switching, context-based retrieval, matched filtering, data encryption, and pattern recognition.

In spite of the rapid progress in the development of optical memories and all-optical processors, to our knowledge there exists no model directly operating at optical communication wavelengths. The current optical devices require electrical-optical signal conversions, which certainly reduce the data-communication speed. Meeting the rapidly increasing demand for high-speed and high-capacity optical communications has made it necessary to eliminate such electrical-optical conversions. However, it remains a challenge to find a suitable medium for storing and processing optical signals at the infrared wavelengths of fiber communication.

In this Letter we explore the feasibility of developing a TDOM that can be operated directly at the communication wavelengths. We choose the  $^4I_{15/2}-^4I_{13/2}$  transition in  $\text{Er}^{3+}:\text{YAG}$  as a candidate for the present study and examine some of its spectroscopic properties that are relevant to time-domain applications.

The  $^4I_{15/2}-^4I_{13/2}$  transition of triply ionized Er is widely used in lasers and optical amplifiers. This transition, occurring at wavelengths near  $1.5 \mu\text{m}$ , suitable for fiber communications, has been studied in glass fiber<sup>9-11</sup> and crystal.<sup>12</sup> These studies focused on either the absorption and the fluorescence of the transition<sup>10-12</sup> or on picosecond photon echo in Er-doped fiber.<sup>9</sup> Little was known about the homoge-

neous dephasing and spectral diffusion in  $\text{Er}^{3+}$ -doped crystal; these properties are critical to the application of TDOM.

We first performed an absorption measurement of  $\text{Er}^{3+}:\text{YAG}$  to resolve the  $^4I_{15/2}-^4I_{13/2}$  transition by using a tunable pulsed dye laser (Quanta Ray PDL-2) that was Raman shifted in a  $\text{H}_2$  gas cell. The laser was operated at a repetition rate of 10 Hz with a pulse width of  $\sim 7$  ns and pulse energy of  $\sim 2$  mJ. The accuracy of the laser wavelength was estimated to be 0.1 nm. The linewidth of the laser was estimated to be  $\sim 4$  GHz. The sample of  $\text{Er}^{3+}:\text{YAG}$  has an  $\text{Er}^{3+}$  concentration of  $\sim 0.1\%$  and was placed either in a closed-cycle refrigerator at  $\sim 7$  K or in a liquid-helium Dewar at  $\sim 1$  K.

The Er ion has an odd number of  $f$  electrons, giving rise to Kramers degeneracy, which can be lifted only by an external magnetic field. We resolved six lines associated with transitions from the lowest Stark level in the  $^4I_{15/2}$  state to six Stark levels of the  $^4I_{13/2}$  state (Fig. 1). Their wave numbers from right to left in Fig. 1 are 6549, 6599, 6606, 6786, 6806, and  $6886 \text{ cm}^{-1}$ . The absorption line at  $6527 \text{ cm}^{-1}$  at  $\sim 7$  K is a hot band from the second-lowest Stark level ( $\sim 22 \text{ cm}^{-1}$ ) in the  $^4I_{15/2}$  state to the lowest level of the  $^4I_{13/2}$  state. At higher temperature, we also observed a hot band from higher Stark levels of the  $^4I_{13/2}$  state. The energy-level diagram of  $^4I_{15/2}$  and  $^4I_{13/2}$  that corresponds to our data is shown in Fig. 2. Our results are in general consistent with research on  $\text{Er}^{3+}:\text{YAG}$  by Ashurov *et al.*,<sup>13</sup> who also observed only six lines for the  $^4I_{15/2}-^4I_{13/2}$  transition at

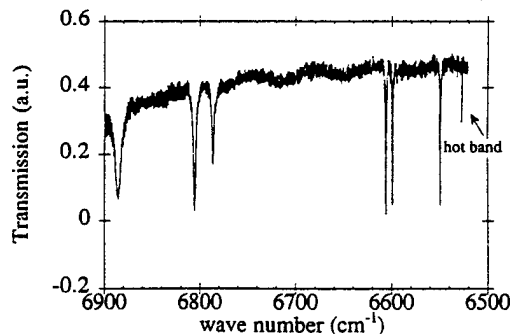


Fig. 1. Transmission spectrum of  $\text{Er}^{3+}:\text{YAG}$  at 7 K.



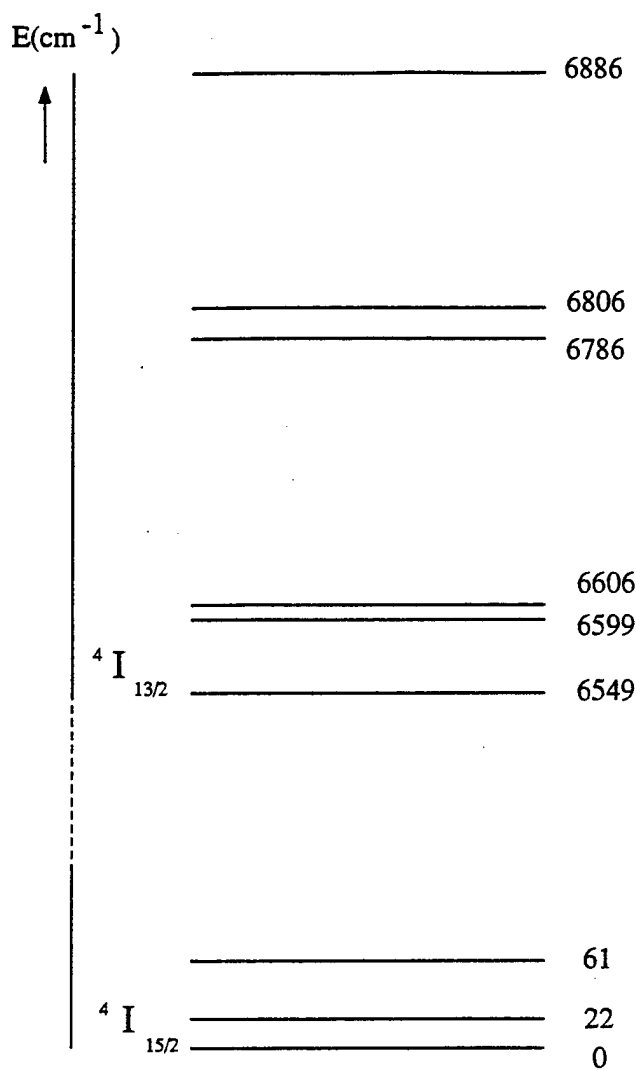


Fig. 2. Energy-level diagram of  $\text{Er}^{3+}:\text{YAG}$  for the  ${}^4I_{15/2}$  and  ${}^4I_{13/2}$  state.

4 K. The data reported by Koningstein and Geusic<sup>14</sup> indicate an additional absorption line  $\sim 91 \text{ cm}^{-1}$  above the highest line in our data, which may be too weak for us to detect.

The rest of our experiment focuses on the transition from the ground state of  ${}^4I_{15/2}$  to the lowest Stark level of the  ${}^4I_{13/2}$  state (i.e.,  $6549 \text{ cm}^{-1}$ , or  $1.527 \mu\text{m}$ ). First the  ${}^4I_{13/2}$  excited-state lifetime was measured with a pump-probe method. We resonantly excited Er ions to that level with an infrared dye laser. We then probed the population of that level by applying another pulsed dye laser to excite the Er ions from the  ${}^4I_{13/2}$  state to the  ${}^4F_{7/2}$  state (at  $20516 \text{ cm}^{-1}$ ) and detecting the fluorescence from the  ${}^4F_{7/2}$ . By delaying the probe pulse with respect to the pump pulse, we measured the  ${}^4I_{13/2}$  state lifetime to be  $\sim 10 \text{ ms}$ , consistent with the result reported by Li *et al.*<sup>15</sup>

The inhomogeneous broadening of the transition was estimated to be  $\sim 20 \text{ GHz}$  from the measured transmission spectrum (Fig. 1). We measured the homogeneous linewidth of this transition by recording

two-pulse echo intensity as a function of excitation pulse separation [shown in Fig. 3(a)]. A fit of the data to a simple exponential function gives a homogeneous dephasing time  $T_2$  of  $\sim 50 \text{ ns}$ . This dephasing time was found to vary little between 1 and 7 K under a magnetic field of less than 100 G.

In our two-pulse echo experiment we use two dye lasers that are similar to the one described for the absorption measurement. The peak intensity of the laser inside the crystal is  $\sim 1 \text{ MW/cm}^2$ . We use the fluorescence lifetime of the  ${}^4I_{13/2}$  excited state to calculate the laser pulse area and take into account that the laser pulse is non-Fourier-transform limited.<sup>16</sup> The estimated pulse area is between  $\pi/8$  and  $\pi/4$ . This area of  $< 1$  was also supported by the experimental observation that the echo intensity was linear to the first laser pulse's intensity and quadratic to the intensity of the second. We also found that reducing the laser power by a factor of 2 had no effect on the decay rate of the echo.

The data plotted in Fig. 3(a) were taken with an external magnetic field of  $\sim 100 \text{ G}$  applied along the  $c$  axis of the crystal. When this external field was increased from 0 to 10 G, the echo intensity quickly increased by a factor of 3. But this increase became saturated when the field was greater than 30 G. On the other hand, the dephasing time did not change when we increased the magnetic field to 100 G. When a magnetic field of  $\sim 3000 \text{ G}$  was applied to the crystal (perpendicular to its  $c$  axis), we observed apparently nonexponential decay of echo, but the dephasing time was not lengthened either.

One of the important parameters governing the performance of the TDOM is the highest temperature at which the storage sample can be operated. To determine this temperature, we measured two-pulse echo intensity at different sample temperatures. At a fixed excitation pulse separation of  $\sim 35 \text{ ns}$ , the echo

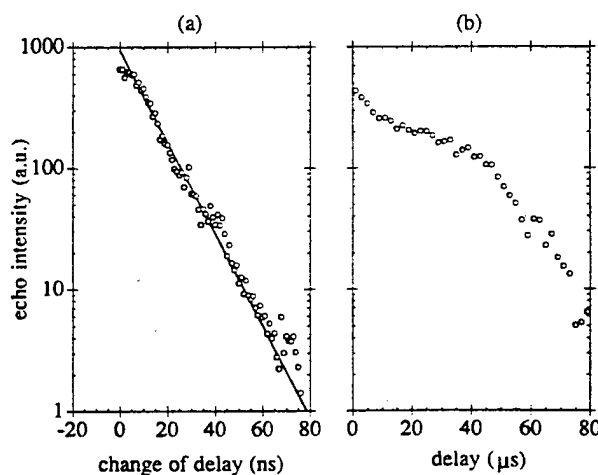


Fig. 3. (a) Two-pulse echo intensity in  $\text{Er}^{3+}:\text{YAG}$  at  $\sim 7 \text{ K}$  under an external magnetic field of  $100 \text{ G}$  as a function of change of excitation pulse separation. Open circles are data, and the solid line is a simple exponential fit. (b) Stimulated photon-echo intensity in  $\text{Er}^{3+}:\text{YAG}$  as a function of the separation between the second and the third excitation pulses. The results were obtained at  $\sim 1 \text{ K}$  under an external magnetic field of  $3000 \text{ G}$ .

intensity gradually decreased by only a factor of 2 from 7 to 11 K. This temperature dependence of  $\text{Er}^{3+}:\text{YAG}$  is considerably weaker than that of other rare-earth-doped crystals, except for  $\text{Eu}^{3+}:\text{Y}_2\text{SiO}_5$  at its  ${}^7F_0-{}^5D_0$  transition.<sup>17</sup>

In addition to performing the two-pulse echo experiments, we also examined three-pulse (or stimulated) photon echo in  $\text{Er}^{3+}:\text{YAG}$ , since it is closely related to the physical processes involved in TDOM and related optical processors. By doing so, we were able to estimate the potential performance of  $\text{Er}^{3+}:\text{YAG}$  in TDOM at 1.527  $\mu\text{m}$ , for example, the maximum storage time, which is often limited by spectral diffusion resulting from ion-host and ion-ion interactions. We carried out the three-pulse stimulated echo experiment under a condition very similar to that of the two-pulse echo experiment. We fixed the separation between the first two excitation pulses at 20 ns and varied that between the second and the third pulses. The results [shown in Fig. 3(b)] show a complicated decay feature, with an initial fast decay followed by a slower decay and then another fast decay. At a delay of 50  $\mu\text{s}$  the echo intensity decreased by a factor of 10 from that at 1  $\mu\text{s}$ . This decay is much faster than the fluorescence lifetime measured in this study, suggesting the presence of rapid spectral diffusion on a microsecond time scale. One possible cause of this fast diffusion is the strong Er-Er dipolar interactions, as suggested by Macfarlane and Shelby.<sup>18</sup>

In conclusion, we have observed for what is believed to be the first time two- and three-pulse echoes at 1.527  $\mu\text{m}$  in  $\text{Er}^{3+}:\text{YAG}$ . Although the fast dephasing of  $\text{Er}^{3+}:\text{YAG}$ , together with its insensitivity to an external magnetic field as observed in our experiments, is less desirable, it poses no significant challenge to the implementation of  $\text{Er}^{3+}:\text{YAG}$  as a time-domain storage medium in most applications. For example, the recently developed swept-carrier technique permits the storage of data strings that are much longer than the dephasing time of a storage material. The lifetime of the spectral grating measured by three-pulse echoes, although it is short, is still adequate for applications such as dynamic optical memory, optical packet buffering, and optical signal processing. The results reported in this Letter open up the possibility of developing TDOM and TDOM-based optical processors operated directly at communication wavelengths. Further improvement of material properties, such as longer dephasing time and less spectral diffusion, could

be accomplished, e.g., by choice of different host materials, reducing Er concentrations, and (or) applying larger external magnetic fields. These efforts have shown success in other rare-earth ions such as Eu and Pr. However, they may not be applicable to Er ions.

This research was supported by the Defense Advanced Research Projects Agency under contract F-49620-95-C-0077. Useful discussions with Robert Leheny and Alan Craig are greatly appreciated.

## References

1. T. W. Mossberg, *Opt. Lett.* **7**, 77 (1982).
2. Y. S. Bai and R. Kachru, "Coherent time-domain data storage with spread-spectrum data pulse," U.S. patent 5,369,665 (November 29, 1994).
3. M. Mitsunaga, R. Yano, and N. Uesugi, *Opt. Lett.* **16**, 1890 (1991).
4. X. A. Shen, E. Chiang, and R. Kachru, *Opt. Lett.* **19**, 1246 (1994).
5. H. Lin, T. Wang, and T. W. Mossberg, *Opt. Lett.* **20**, 1658 (1995).
6. Y. S. Bai, W. R. Babbitt, N. W. Carlson, and T. W. Mossberg, *Appl. Phys. Lett.* **45**, 714 (1984).
7. X. A. Shen, Y. S. Bai, and R. Kachru, *Opt. Lett.* **17**, 1079 (1992).
8. M. Zhu, C. M. Jefferson, and W. R. Babbitt, in *Spectral Hole-Burning and Related Spectroscopies: Science and Applications*, Vol. 15 of 1994 OSA Technical Digest Series (Optical Society of America, Washington, D.C., 1994), p. 392.
9. Y. Silberberg, V. L. da Silva, J. P. Heritage, E. W. Chase, and M. J. Andrejco, *IEEE J. Quantum Electron.* **28**, 2369 (1992).
10. W. L. Barnes, P. R. Morkel, L. Reekie, and D. N. Payne, *Opt. Lett.* **14**, 1002 (1989).
11. E. Desurvire and J. R. Simpson, *Opt. Lett.* **15**, 547 (1990).
12. C. Li, C. Wyon, and R. Moncorge, *IEEE J. Quantum Electron.* **28**, 1209 (1992).
13. M. K. Ashurov, Y. K. Voronko, V. V. Osiko, A. A. Sobol, B. P. Starikov, M. I. Timoshechkin, and A. Y. Yablonskii, *Phys. Status Solidi A* **35**, 645 (1976).
14. J. A. Koningstein and J. E. Geusic, *Phys. Rev. A* **136**, 726 (1964).
15. C. Li, J.-C. Souriau, and R. Moncorge, *J. Phys. IV (Paris)* **C7**, 371 (1991).
16. T. W. Mossberg, R. Kachru, S. R. Hartmann, and A. M. Flusberg, *Phys. Rev. A* **20**, 1976 (1979).
17. Y. Zhang and R. Kachru, *Appl. Opt.* **35**, 6762 (1996).
18. R. M. Macfarlane and R. M. Shelby, *Opt. Commun.* **42**, 346 (1982).

**APPENDIX C**

**TIME-DOMAIN HOLOGRAPHIC DIGITAL MEMORY**

## Time-Domain Holographic Digital Memory

Xiao A. Shen, An-Dien Nguyen, John W. Perry,\*  
David L. Huestis, Ravinder Kachru†

An optical storage technique based on time-domain holography for the rapid recording and readout of page-formatted digital data is demonstrated. Storage of 356 kilobits of data was achieved at a single spatial location in a rare-earth-doped crystal. The digital data were recorded and accurately retrieved at a peak rate of 300 megabits per second without the use of error-correcting codes. The system's raw bit error rate is about  $10^{-7}$ . This low bit error rate was achieved by a detection scheme for extraction of binary data. These results have implications for dynamic optical memory.

**H**olographic memories, once considered a storage device of the distant future, have come much closer to reality. Instruments that make use of holographic approaches to data storage have been developed and tested for applications such as the identification of fingerprints (1). Use of spatial holography to store page-formatted digital optical data in computer-based applications has also been explored, and the results are promising (2-4). The memories are believed to be superior to existing technologies, with key features including ultrahigh storage density, rapid data transfer, short data access times, and exceptional reliability.

Although much progress has been achieved in some key areas of holographic data storage, several major technical impediments remain, restricting its application in a broad area, as was promised initially. The most noticeable obstacle has been the slow recording rate of conventional holographic techniques, which record spatial interference patterns generated by two temporally co-existing laser beams. The recording requires, in addition to laser excitation, subsequent electron diffusion in storage materials, as in

the case of photorefractive memory, for example. Such processes limit photorefractive technology to applications that are not input intensive, such as memory that is written only once. Success in developing high-performance input-output (I/O)-intensive holographic memories, such as page-oriented dynamic optical random access memory, will require the development of much higher recording speeds while maintaining high storage densities and low bit error rates, the latter being a benchmark for the quality of stored data.

Time-domain holographic memory has emerged as an excellent candidate for such I/O intensive applications (5, 6). This memory not only has features common to conventional spatial holographic recording, such as high capacity and high degree of parallelism, but also some that are complementary to conventional holography, including fast page recording speed and modest laser power requirement. Recent experiments (6) show that an exposure time of several microseconds and a peak laser power of less than 200 mW are sufficient to record a high-resolution binary image with the time-domain technique.

Historically, the time-domain holographic approach evolved from an optical transient phenomenon known as stimulated photon echoes (7). It is a time-domain or, equivalently, a spectral-domain version of holographic recording. Like conventional

---

Molecular Physics Laboratory, SRI International, Menlo Park, CA 94025, USA.

\*Permanent address: Department of Computer Science and Mathematics, Carleton College, Northfield, MN 55057, USA.

†To whom correspondence should be addressed. E-mail: kachru@mplvax.sri.com

holography, this technique stores data as holograms by using a reference beam and a data beam. These two beams interfere at a recording medium, causing a change of the optical properties of the medium. Unlike in spatial holography, the reference and data beams appear in the form of short laser pulses and do not overlap temporally. In most recording schemes developed to date, the reference pulse precedes the data pulse by several nanoseconds to several microseconds to provide, in addition to a spatial reference, a temporal reference for the recorded holograms (Fig. 1). The interference generated by these two temporally distinct laser pulses occurs in both spectral and spatial domains, giving rise to four-dimensional holograms (8).

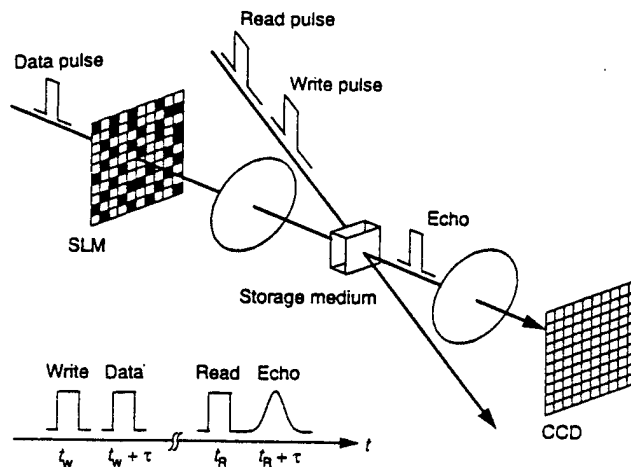
The spectral interference of the two pulses is recorded in a storage medium [which is often a rare-earth-doped solid such as  $\text{Eu}^{3+}:\text{Y}_2\text{SiO}_5$  or  $\text{Pr}^{3+}:\text{YAG}$  (YAG, yttrium-aluminum-garnet)] by laser excitation. Ions such as  $\text{Eu}^{3+}$  and  $\text{Pr}^{3+}$  that are responsible for data recording are resonantly excited by the laser pulses to form population gratings that resemble the Fourier spectra of the pulse pair (Fig. 2). These gratings in a carefully chosen material can persist for several hours to perhaps several days at cryogenic temperatures because the recorded information is actually stored as population modulation of hyperfine levels in the ground state (6). Because the grating is a direct result of resonant excitation and requires no secondary process, its formation is instantaneous and requires modest laser power; the data recording is therefore inherently fast and efficient, giving rise to high data transfer rates, fast access times, and short latency. These features are ideal for applications such as a dynamic memory.

Data stored as population gratings are retrieved by illuminating the sample with another laser pulse known as the read pulse (Fig. 2), which reconstructs the object field as in conventional holography. However, unlike in conventional holography, the reconstructed field appears as an emitted laser pulse and is temporally distinct from the read pulse, just as in case of recording. For a given temporal separation  $\tau$  between the write and data pulses, the reconstructed pulse will occur a time  $\tau$  after the arrival of the read pulse (Fig. 1) and has spatial features identical to those of the stored data pulse. This delayed radiation is often referred to as photon echoes. Mathematically, the Fourier transforms of the echo and three input pulse electrical fields  $\vec{E}$  are related in the following manner

$$\vec{E}_e(\nu) \propto \vec{E}_W^*(\nu) \vec{E}_D(\nu) \vec{E}_R(\nu) \quad (1)$$

where the subscripts e, W, D, and R denote echo, write, data, and read pulses, respec-

Fig. 1. Time-domain holographic recording scheme. The insert shows the order in which the write, data, read, and reconstructed pulses occur.



tively, and  $\nu$  denotes the frequency. Because the echo is a replica of the data pulse both spatially and temporally, the peak readout rate (the number of bits per echo) is identical to the peak recording rate (the number of bits per data pulse) in a time-domain digital memory.

The material we chose to demonstrate this recording scheme was crystalline  $\text{Eu}^{3+}:\text{Y}_2\text{SiO}_5$  (0.1 atomic %, 7 mm thick). We used its  ${}^7\text{F}_0-{}^5\text{D}_0$  transition at site 1 ( $\sim 579.88$  nm), which has an inhomogeneously broadened linewidth of  $\sim 4$  GHz and a dephasing time of  $\sim 2$  ms (9). The product of the two parameters gives the theoretical upper bound for the storage capacity per spatial location as a result of the presence of the wavelength dimension. This material has two optically equivalent sites for the transition; the other site (site 2) has a comparable linewidth and dephasing time (9), making the material a good candidate for high-capacity applications. During the experiments, the crystal was kept at a temperature of about 4 K in a flowing He-vapor cryostat.

Digital data pages, each of which contained 3360 bits of data, were generated by illuminating a spatial light modulator (SLM) (10) with laser pulses as short as

$11.2 \mu\text{s}$  (11), giving rise to a maximum peak (burst) recording rate of 300 megabits per second. Each page was stored in a distinct, narrow ( $\sim 500$  kHz) frequency channel (12) within the inhomogeneously broadened absorption line by wavelength-division multiplexing (WDM). The separation between two adjacent channels was chosen to be  $\sim 800$  kHz. There are distinct advantages to WDM (13): (i) Recording and retrieval can be accomplished without the use of any moving parts for laser beam steering, so that it is inherently reliable and often provides short access times (12); (ii) there is no significant effect on diffraction efficiency; and (iii) each data page can be recorded in an identical manner, eliminating the need for scheduled or incremental recording, as is used in angular-division multiplexing (14).

The retrieved data were captured by an intensified charge-coupled device (CCD) camera and subsequently digitized by a frame grabber (15). The SLM and CCD operated at the video rate (30 frames per second, which is the maximum frame rate allowed for the devices), and the resulting digitized data were transferred at the same speed to a computer's dynamic memory. At the present time, the SLM limits the sustainable recording speed to

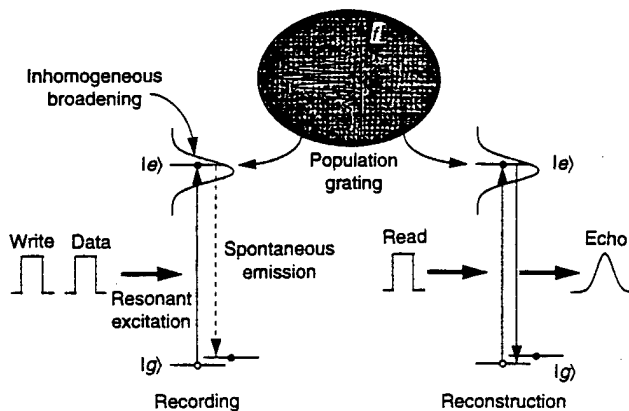
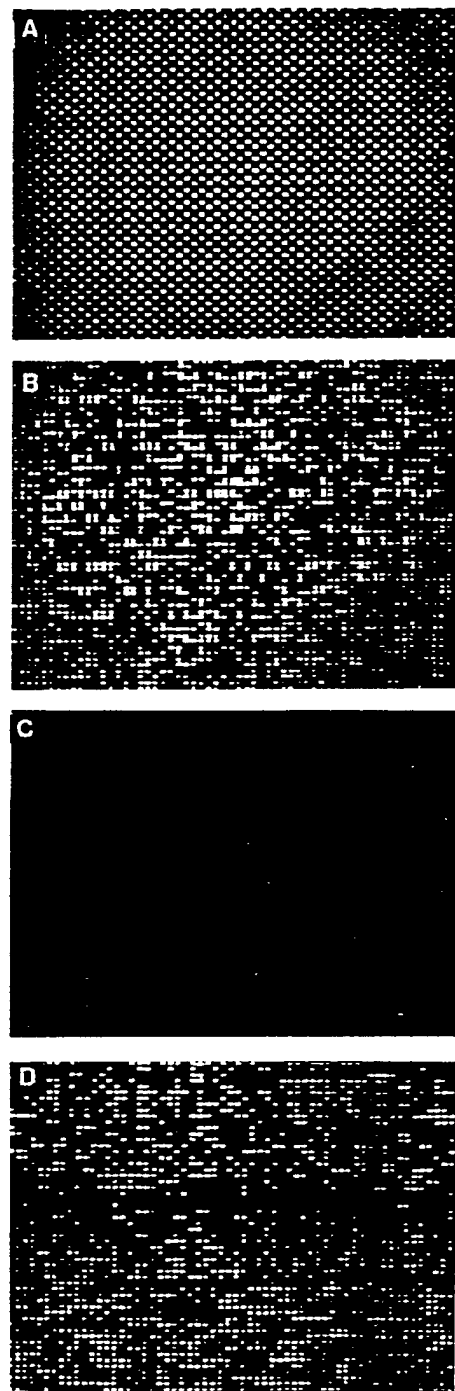


Fig. 2. Schematic of the mechanism for the formation of the population grating and echoes under the laser excitations. Symbols  $|g\rangle$  and  $|e\rangle$  denote the ground and excited states of an electronic transition, respectively, and the vertical labeled  $f$  represents the frequency.

~110 kilobits per second, substantially lower than the burst rate of 300 megabits per second permitted by the storage material; however, this limit is not fundamental. High-speed



**Fig. 3.** (A) Input data image after transmission through the  $\text{Eu}^{3+}:\text{Y}_2\text{SiO}_5$  sample. (B) Reconstructed image after storage in  $\text{Eu}^{3+}:\text{Y}_2\text{SiO}_5$  for 200  $\mu\text{s}$ . (C) Image reconstructed under the same conditions as in (B) but with weak overall intensity. (D) Image reconstructed 5 min after the completion of recording. In (A) through (C), the length of the data pulse was 11.6  $\mu\text{s}$ , and that in (D) was 50  $\mu\text{s}$ . These times correspond to I/O rates of 300 and 67 megabits per second, respectively.

SLMs with a full frame rate of 3 kHz are commercially available; ones with higher speeds are being considered for development. Semiconductor laser arrays may be used in the future to compose binary digital pages without the need of SLMs. Such devices will have a single-channel modulation rate sufficiently high (in excess of 1 GHz) to match the burst rate set by the page exposure time.

In digital memories, one important parameter determining the memory's performance is the bit error rate (BER), which measures how often an error bit occurs on average. This parameter is closely related to other performance parameters of the system, such as storage capacity, data transfer rates, and data access times. In general, for a given system, attempting to reduce the BER leads to a decrease of storage capacity or data transfer rate,

or both, because a low BER requires high signal-to-noise ratios, which implies the use of large bit dimensions in the case of parallel recording. For a given frame size, it translates into a decrease of the data transfer rate.

For an optical storage system operating at high I/O speeds with low laser power illumination, the retrieved data are often at a signal level that is limited by shot noise, which is a result of the quantum nature of photons. For page-formatted recording, the process is further complicated by the non-uniform illumination of an SLM. Because of these undesired conditions associated with a low photon budget, such a system often exhibits large page-to-page fluctuations and intrapage variations.

Figure 3A shows a sample input page used in data recording. Spatial variation of the intensity is apparent. This variation reflects the spatial beam mode of the addressing laser, contributing partially to the spatial signal variations within a page discussed earlier. The other contributions include shot noise.

The page-to-page fluctuation is often more noticeable in the retrieved data because it is magnified by less-than-ideal recording and readout conditions. Figure 3, B and C, show two retrieved pages that represent the brightest and dimmest among a total of 100 pages recorded in an experiment. They are single readout events with no signal averaging. The intensity difference between the two pages is >300%, which is mainly caused by the frequency instability of the laser system (12).

Examination of the histogram of all 100 pages (totaling 336 kilobits of data) reveals that the intensity distributions of the 1's (or ON's) and 0's (or OFF's) partially overlap (Fig. 4A). If a single threshold were used to determine all of the data bits, it would lead to a BER as large as  $10^{-3}$ , which is not suitable for any storage application.

The broad distribution curves in Fig. 4A are mainly a reflection of the interpage intensity fluctuations and intrapage variations. The broadening also includes cross talk between neighboring 1's and 0's. If these intensity variations and cross talk were removed, the distributions for both 1's and 0's would follow closely scaled Poisson distributions, which has been confirmed experimentally for known images. Under this condition, a single threshold can be obtained for the whole page with knowledge of the average of the intensities of 1's and 0's only. This finding allows us to develop the following scheme to rapidly and accurately read page-formatted binary data that have large intrapage intensity variations and large interpage fluctuations.

We use recently determined data bits to obtain a local threshold for the next bit under consideration. The local region is

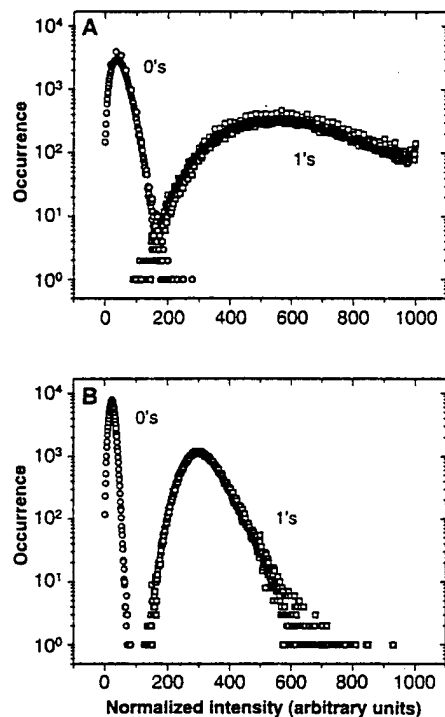


**Fig. 4.** (A) Histogram showing the intensity distributions of 0's and 1's that were retrieved from the time-domain memory. (B) Normalized histogram obtained after applying the local threshold technique. In obtaining these results, we used a peak recording rate of 300 megabits per second. The 100 pages were wavelength-division multiplexed at a single storage cell measuring about 1.0 mm by 1.0 mm by 7.0 mm at a rate of 30 frames per second with a total recording time of ~3.3 s. All of the pages used here were obtained from the same experiment. For convenience, each page used for BER analysis was retrieved after being transferred to the memory for 200  $\mu\text{s}$ . The use of short storage time prevented the undesired page-to-page fluctuation caused by the slow frequency drift of our laser. An example of long-term storage is shown in Fig. 3D. The echo (or "diffraction") efficiency for the short-term storage was measured to be  $\sim 5 \times 10^{-3}$ .

chosen in such a way that it occupies an area that is small enough so that the illumination is approximately uniform yet large enough to have a sufficient number of bits for an adequate average. Under such a condition, a threshold can be derived from the scaled Poisson distributions to accurately determine the state of the bit, provided that the intensity within a page varies smoothly. We adopted the following formula for the threshold

$$I_{\text{thr}} = I_0 + p\sqrt{I_0} + q[(I_1 - p\sqrt{I_1}) - (I_0 + p\sqrt{I_0})] \quad (2)$$

where  $I_0$  and  $I_1$  are the average intensities of 0's and 1's,  $q$  is a weighting factor (chosen empirically to be  $1/3$ ), and  $p$  is a measure of at how many standard deviations above  $I_0$  and below  $I_1$  we can place the threshold. Here, we use  $p = 11$ . The optimum numbers used in averaging were found to be 4 for 0's and 8 for 1's.

Initial values of  $I_0$  and  $I_1$  are needed to jump start the analysis of each page. This is accomplished by permanently setting to 0 four known bits at the corners of a  $4 \times 4$  region in the center of the SLM, where the signal-to-noise rate is largest. We average the 4 bits to estimate  $I_0$ . A crude estimate for  $I_1$  can be obtained by averaging the intensities of the remaining 12 unknown bits. The threshold for the block is then calculated from Eq. 2 by assuming the block intensity  $I_{\text{block}} = (I_0 + I_1)/2$ , which implies an equal number of 1's and 0's in the block. This approach yields a BER of  $10^{-6}$  for the 12-bit central region, or equivalently, a  $10^{-5}$  probability of having an error bit per page.

We then continue this analysis process by spiraling outward from the center of a page toward the edges, with the intensity decreasing gradually as the analysis proceeds. The neighboring 1's and 0's are stored in two separate register arrays and updated in a first-in-first-out manner to obtain their running averages. Thus, each data bit is determined in real time with the use of Eq. 2. In comparison to existing schemes for reading page-formatted digital data (2, 16), this automatic threshold calibration technique uses no coding bits and requires no mathematical iteration. These advantages lead to a significant increase in the readout rate, which is ideal for high-speed applications.

Using this approach, we repeated the above experiment and obtained a histogram for the same 100 pages used earlier (Fig. 4B). This histogram was normalized to the respective threshold of each data bit and shows two clearly separate distribution curves. The separation is  $\sim 40\%$  of the full width of the distribution for 0's. This large separation suggests an effective increase of the system's dynamic range by  $\sim 40\%$ . The raw BER is esti-

mated to be  $\sim 10^{-7}$ . We further verified this number by repeating the experiment 10 times: The two distribution curves in the resulting histogram remained separate.

According to our BER measurement, our current storage system is capable of recording close to 10 megabits of digital data without generating an error bit. To demonstrate it, we stored a high-resolution black-and-white photograph of Albert Einstein (Fig. 5A). The digitized photograph contains 106 pages, totaling 356 kilobits, of digital data. Figure 5B shows the reconstructed photograph after being copied to and read back from the memory. The entire photograph was stored at a single spatial location in  $\text{Eu}^{3+}:\text{Y}_2\text{SiO}_5$  using WDM with a peak recording speed of 300 megabits per second, and no error correcting code of any kind was used. The total material bandwidth used was only  $\sim 85$  MHz.

Because  $\text{Eu}^{3+}:\text{Y}_2\text{SiO}_5$  has two equivalent optical sites with a total of  $\sim 8$  GHz inhomogeneous bandwidth, 85 MHz represents only  $\sim 1\%$  of the available storage capacity at this location. In principle, 100 such photographs can be wavelength multiplexed at this spatial location, which implies a total raw capacity of  $\sim 4.5$  megabytes. Taking into account the active storage volume used, the projected density is  $\sim 6 \times 10^8$  bits per cubic centimeter.

The above estimates were based on simple extrapolation of our current experimental results, which were obtained under conditions that were far from optimum (15); therefore, these numbers do not represent the fundamental limits of the stor-

age system. The projected capacity can be increased substantially by using, for example, a matched SLM, CCD, and frame grabber (3). Furthermore, the use of SLMs with lower insertion loss would also increase the storage density because higher spatial resolution can be achieved with a high-power addressing beam. Currently, SLMs with an insertion loss of  $< 20\%$  are commercially available. With the rapid advance of peripheral devices, such as SLMs and CCD cameras, the achievable storage capacity is likely to be several orders of magnitude greater than what is projected here.

The recording and readout speeds would also be increased by the use of a SLM with lower insertion loss. We estimate that the length of the data pulse can be reduced by a factor of 5 without loss of signal strength by using a SLM with 20% insertion loss. This adjustment would allow an I/O rate of  $\sim 1.5$  gigabits per second. Furthermore, by using matched SLMs and CCDs, an I/O rate in excess of 10 gigabits per second should be achievable without any penalty in raw BER.

Parallel digital data storage making use of the time-domain approach could be developed into a high-performance page-oriented dynamic optical memory. As the technology for parallel data access becomes more mature, this time-domain holographic approach along with other optical holographic storage techniques (such as photorefractive memory) may fulfill their long-awaited promise for high-speed, high-density data storage. A number of issues still need to be addressed before this

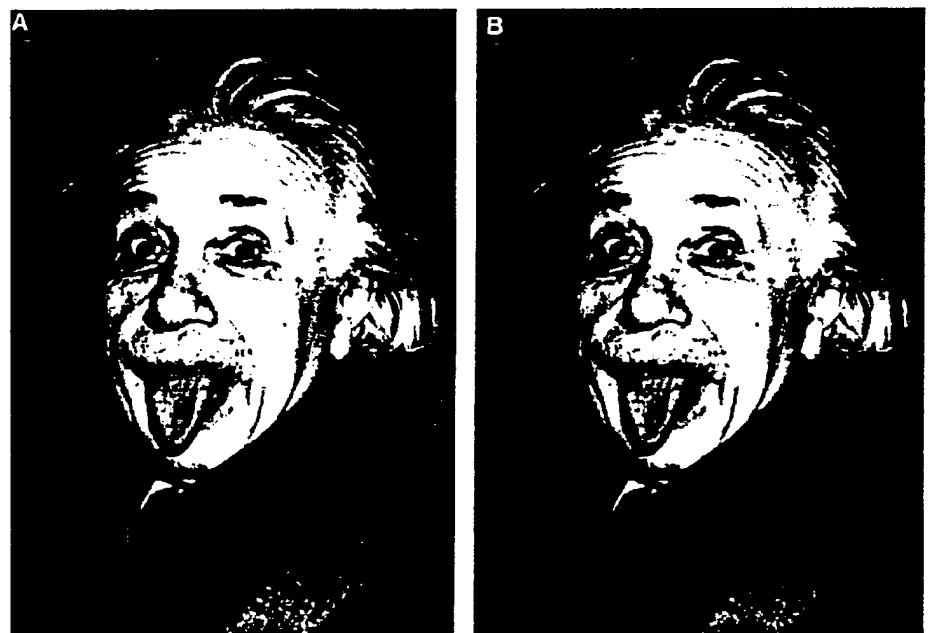


**Fig. 5.** (A) Digitized photograph displayed using its original binary data. (B) Same photograph obtained after the binary data was transferred to and then recalled back from the time-domain memory. [Reprinted with permission from UPI/Corbis-Bettman]